CALIFORNIA STATE UNIVERSITY SAN MARCOS

THESIS SIGNATURE PAGE

THESIS SUBMITTED IN PARTIAL FULFILLMENT
OF THE REQUIREMENTS FOR THE DEGREE

MASTER OF SCIENCE

IN

BIOLOGICAL SCIENCES

THESIS TITLE: **IDENTIFYING POTENTIAL BIOMINERALIZATION GENES IN THE COCCOLITHOPHORID *GEPHYROCAPSA OCEANICA***

AUTHOR: Estela Nicolasa Carrasco

DATE OF SUCCESSFUL DEFENSE: December 13, 2016

THE THESIS HAS BEEN ACCEPTED BY THE THESIS COMMITTEE IN PARTIAL FULFILLMENT OF THE REQUIREMENTS FOR THE DEGREE OF MASTER OF SCIENCE IN BIOLOGICAL SCIENCES.

Dr. Betsy Read THESIS COMMITTEE CHAIR	Betsy Read SIGNATURE	12/13/16 DATE
Dr. Julie Jameson THESIS COMMITTEE MEMBER	Julie Jameson SIGNATURE	12/13/16 DATE
Dr. Jose Mendoza THESIS COMMITTEE MEMBER	 SIGNATURE	12/13/16 DATE
William Whalen THESIS COMMITTEE MEMBER	 SIGNATURE	13 DEC 2016 DATE

Identifying potential biomineralization genes in the coccolithophorid *Gephyrocapsa oceanica*

By

Estela Nicolasa Carrasco

Research Thesis Submitted for the Master's Degree in

Biological Sciences

Department of Biological Sciences

California State University, San Marcos

Fall, 2016

TABLE OF CONTENTS

Acknowledgements

I am using this opportunity to express my gratitude to everyone who supported me throughout the course of this thesis project. Firstly, I would like to express my sincere gratitude to my advisor Dr. Betsy Read for expert advice, continuous encouragement, and extraordinary support throughout this challenging thesis project. Besides my advisor, I would like to thank the rest of my thesis committee members: Dr. Julie Jameson, Dr. Jose Mendoza, and William Whalen, for their insightful comments, guidance, and encouragement. Also, a special thank you to Dr. William Kristan for providing statistical advice and to Dr. Deborah Kristan and Dr. Thomas Spady for their support and assistance with paperwork needed to continue my thesis. To Xiaoyu Zhang from Computer Science & Information Systems for the bioinformatics work.

Secondly, I thank my fellow lab mates: Patricia Byrne, Steven Castro, Aaron Hernandez, and Tien Nguyen for all the long hours spent helping with experiments. I am also grateful to Andrew Segina and Chrystal Schroepfer for being mentors and friends. To Christina Fuller for her continuous encouragement, friendship and for providing a sympathetic ear during hard times.

Finally, I would like to thank my family. A special thanks to my asian sister Joan Choi, your love, encouragement, and support since high school has made this journey possible. To my husband Ben B. Shen, your love and continuous encouragement has kept me sane throughout this project. To my sister and her husband, Justina and Delfino Avendaño, thank you for always supporting my dreams for higher education. To my nephews, the Avendaño kids (Ediberto, Pedro & Daniel), thank you for always providing distractions and making life fun. My brother, Ernesto and his family for their support. To my parents, Nieves Estrada and N. Antolin Carrasco, thank you for your unconditional love and support over the years. Finally, this thesis is dedicated to the memory of Ock R. Choi and my brother Ramon R. who could not see this thesis completed. This is for you, I hope you are proud of me.

ABSTRACT

The Prymnesiophyceae class includes the order Isochrysidales, which consists of coccolith forming sister-species *Gephyrocapsa oceanica*, *Emiliania huxleyi,* and the non-coccolith forming species *Isochrysis galbana*. These coccolithophores form their coccoliths through the process of biomineralization. The molecular mechanisms and genes involved in the process remains unclear. The aim of this study was to identify potential genes involved in biomineralization in the species *E. huxleyi* and *G. oceanica* and compare them to the non-coccolith forming species *I. galbana* by transcript profiling using a high-throughput RNA-sequencing (RNA-seq) method. The transcriptome profiles were generated for cells grown in calcium replete conditions and calcium deplete conditions, with or without the addition of sodium bicarbonate. Physiological parameters including cell growth, rate of calcium uptake and photosynthesis further supported the evidence that photosynthesis and calcification are independent processes. The effects of calcium replete conditions and calcium deplete conditions on calcification and coccolith morphology were monitored via SEM. The data further supported the finding that cells grown in calcium deplete conditions have fragments of coccoliths while cells in calcium replete conditions have well-formed and intact coccoliths. The RNA-seq identified 295 differently expressed genes using negative binomial distribution to compare transcript levels for all three species grown under calcifying 9 mM Ca^{2+} and 0 mM Ca^{2+} conditions. Real time RT-PCR was used to independently validate the differential expression of 21 potential calcifying genes. Real time RT-PCR validated a total of 17 out of 21 differentially expressed genes, for which 6 were considered significantly up-regulated and 11 were considered significantly down- regulated. *G. oceanica* real time RT-PCR analyses independently validated 12 out of 21 genes (57%), while *E. huxleyi* analyses validated 13 out of 21 genes (61%) of the differentially expressed genes when compared to the RNA-seq data**.**

Keywords: *Gephyrocapsa oceanica, Emiliania huxleyi, Isochrysis galbana,* Isochrysidales, biomineralization, coccolith, coccolithophorid, scanning electron microscopy, high-throughput RNA sequencing, transcriptome profiling, real-time RT-PCR.

Introduction

Coccolithophorids

Coccolithophores are unicellular marine algae that have $CaCO_3$ exoskeletons (Ozaki et al., 2004). They belong to the phylum Haptophyta and are known for their distinctive calcium shell coverings known as coccoliths. More than 200 species of coccolithophores have been identified (Holligan et al., 1993). *Emiliania huxleyi (E. huxleyi)* is the dominant coccolithophore and forms large blooms throughout the world's oceans (Brown et al., 1994). Due to its abundance and widespread distribution, coccolithophores, in particular *E. huxleyi* and *Gephyrocapsa oceanica* (*G. oceanica)*, play a role in the ocean's carbon cycles because of their ability to use inorganic CO_2 for both photosynthesis and biomineralized products (Westbroek et al., 1993).

The coccolithophore's unique ability to produce coccoliths have made them ideal targets to study when looking at biomineralization processes. Understanding the underlying mechanisms that control biomineralization in coccolithophores may shed light on the different aspects of biomineralization strategies and processes used by other organisms. New advancements in sciences and research have brought together scientists from cross-disciplines to study biomineral formation (Weiner and Dove, 2003). Understanding the processes of Biomineralization has the potential to impact materials science, medicine and dentistry (Mann, 2001). Characterizing the molecular mechanisms that govern calcification in *E. huxleyi* will help advance the study of pathological mineralization such as kidney stone formation, dental calculus, and osteoporosis (Giachelli, 2005; Mann, 2001). The nanoscale architecture and light reflecting properties of the coccoliths have also attracted the attention of materials scientists for novel

applications relating to biomedical, optoelectronic, nanotechnology and telecommunication devices (Gordon and Parkinson, 2005).

Isochrysidales

The phylum Haptophyta is comprised of unicellular photosynthetic flagellates that possess a unique microtubule supported appendage called a haptonema that resides between the two flagella and is used for food capture (Edvardsen et al., 2000). The phylum consists of two classes: the Pavlovophyceae and Prymnesiophyceae. In the Prymnesiophyceae class, there are four orders: Phaeocystales, Prymnesiales, Isochrysidales and Coccolithales. The species of interest for this study are within the Isochrysidales order, the main order within the Prymnesiophyceae class and consists of two coccolith forming species, *E. huxleyi* and *G. oceanica* and the non-coccolith bearing species *Isochrysis galbana* (*I. galbana*) (Edvardsen et al., 2000). All three species share a number of distinguishing traits including having a small or nonexistent haptonema, two small flagellar apparatuses and a small organic scale layer external to the plasmalemma (Edvardsen et al., 2000). There is also a distinctive structure underneath the plasmalemma which is a very thin membranous sheet in the peripheral endoplasmic reticulum (ER), not been found in other members of the Haptophyta phylum and appearing to be synapomorphic to this clade (Inouye, 1997). Coccolithophores have a heteromorphic life cycle that include a haploid (motile) and diploid (nonmotile) stage (Green et al., 1996; Klaveness, 1972). The coccolith bearing species *E. huxleyi* and *G. oceanica* are similar in that during the nonmotile stage they bear calcium carbonate cell coverings. The non-coccolith bearing species *I. galbana* has unmineralized scales covering its cell body, resembling the motile phase of *G. oceanica* and *E. huxleyi* (Edvardsen et al., 2000).

The similarities in the morphological structure and life cycles of the three Isochrysidales species, *E. huxleyi*, *G. oceanica* and *I. galbana*, suggest a close phylogenetic relationship as illustrated in Figure 1 (Edvardsen et al., 2000). *E. huxleyi* and *G. oceanica* are considered sister species because they share genetically identical Ribulose-1,5-bisphosphate carboxylase/oxygenase large subunit (rbcL) (Fujiwara et al., 1994) and nearly identical 18s rDNA gene sequences. The 18s rRNA sequences that differ by a single nucleotide. These data together with the striking morphological similarities strongly suggest that *E. huxleyi*, *G. oceanica* and *I. galbana*, belong to the same taxonomic group (Edvardsen et al., 2000).

Although fossil records indicate that *E. huxleyi* and *G. oceanica* separated from each other 200,000-1,000,000 years ago, they are regarded by some as morphospecies because they share the same intracellular structures, life cycles and strikingly similar coccolith morphologies (Fujiwara et al., 1994). Both *E. huxleyi* and *G. oceanica* form large blooms and are responsible for producing calcium carbonate deposits in the world's oceans (Rhodes et al., 1995). *G. oceanica* coccospheres ranges in size from 6 to 10 μm while coccoliths range from 3.5 to 6 μm long. Meanwhile *E. huxleyi* produces coccolith that are around 2.5 μm in diameter. *E. huxleyi* is found everywhere from cold temperate to tropical seas, whereas *G. oceanica* is restricted to water temperatures ranging from 12^{o}C to 30^{o}C (Paasche, 2001; Bollmann, 1997). *G. oceanica* is more abundant in tropical and subtropical waters (Bollmann, 1997).

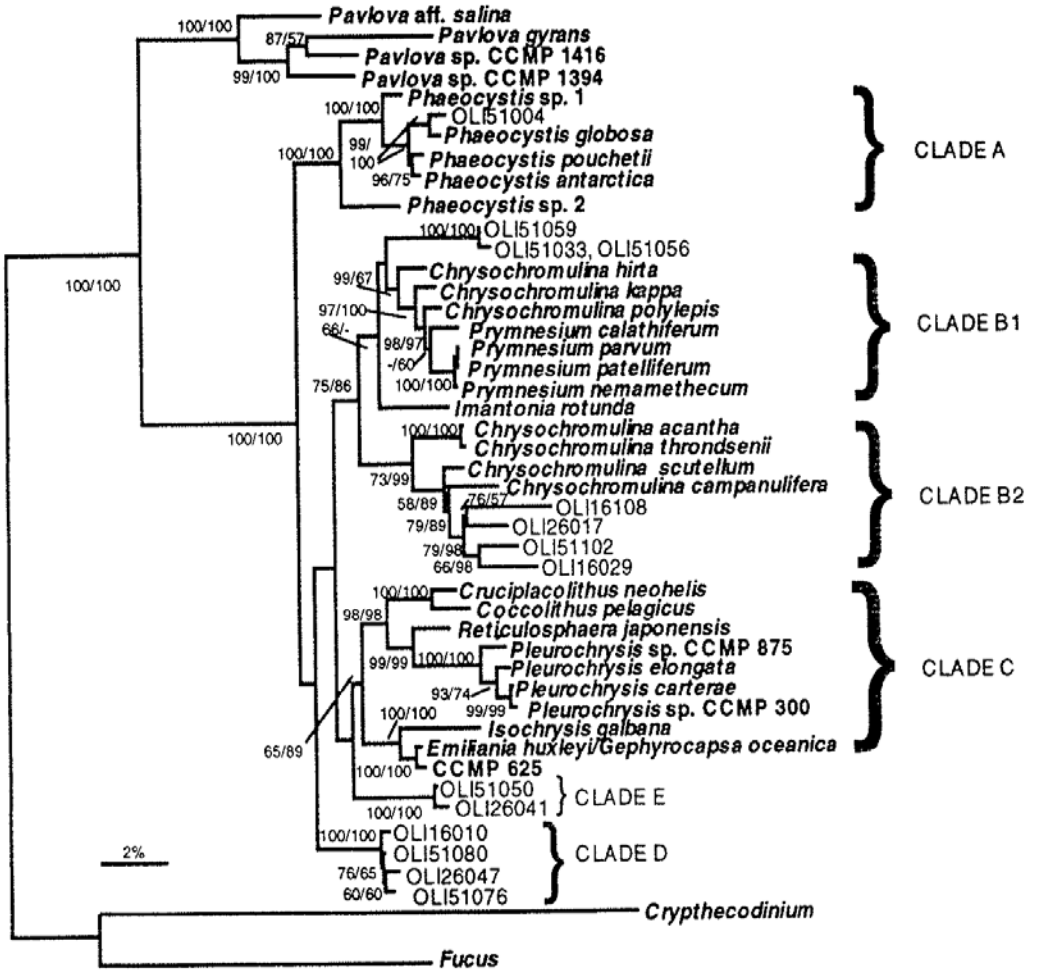

Figure 1: A phylogenetic tree of the haptophyte algae based on nucleotide sequences of the 18S rRNA gene. References from Edvardsen et al., 2000.

Biomineralization

Biomineralization is the process by which organisms form and deposit minerals (Weiner and Dove, 2003). Biomineralization is common throughout the three domains of life and occurs in higher vertebrates and microorganisms alike (Nagasawa et al., 2004). A variety of minerals including calcium carbonate, calcium phosphate, sulfates, sulfides and silica are used for biomineralization purposes (Livingston et al., 2006). Calcium carbonate minerals are the most prevalent among different taxa with some examples including calcite,

magnesium calcite, aragonite, vaterite and monohydrocalcite (Weiner and Dove, 2003). Organisms produce biomineralized structures for different reasons such as structural support, defense, and/or the storage of minerals. Examples of biominerals can be found in mollusk shells, the exoskeletons of crustaceans, and coccoliths in marine algae (Nagasawa, 2004). Although the purpose of biomineralization in coccolithophores is not yet known, it is hypothesized that these coccoliths might provide a protective barrier against predation and chemical or physical shock. Others speculate that coccoliths assist in regulating buoyancy, which would assist with the need to stay within the photic zone and provide an advantage in nutrient absorption by affording the ability upon shedding and amassing coccoliths, to move up and down in the water column (Young, 1994). It is also suggested that coccolith formation involves HCO_3 influx, which in turn leads to an internal supplementation of CO_2 for photosynthesis (Sikes and Wilburn, 1982). It has also been argued that calcification is linked to photosynthesis by providing a source of carbon dioxide to potentially reduce the energy cost (Young, 1994).

Biomineralization processes fall into one of two categories: biologically induced or matrix-mediated biomineralization (Young et al., 1999; Young and Henriksen, 2003). In a biologically induced mineralization system, by-products of metabolic activities that are secreted cause nucleation and growth of minerals in an uncontrolled manner. In this instance, the organism or biological system has little control over the types of minerals formed. In contrast, biomineralization that occurs in a biological-matrix-mediated manner takes place intracellularly and is strictly controlled by macromolecules including proteins, lipids and polysaccharides. Matrix-mediated processes typically occur within a specialized compartment that affords tight control over crystal nucleation, growth, and morphology

(Young et al., 1999). When biomineralization occurs in biological systems, a specialized zone or intracellular compartment is often required to regulate and maintain supersaturated ion concentrations for crystal nucleation and growth (Weiner and Dove, 2003). This intracellular vesicle in coccolithophores is known as the coccolith vesicle, which resides close to the nucleus. In the coccolith vesicle the following calcification reaction occurs: $Ca^{2+} + 2HCO_3^- \rightarrow CaCO_3 + CO_2 + H_2O$ (Sikes et al., 1980). Through this process, coccolithophorids convert inorganic carbon into organic and biomineralized product for coccolith formation (Sorrosa et al., 2004).

Biomineralization in *E. huxleyi* and *G. oceanica*

Coccolith formation in *E. huxleyi* and *G. oceanica* begins with the nucleation of a proto-coccolith ring of simple crystalline units around an organic base-plate (Henriksen and Stipp, 2009; Mann, 2001). The golgi-derived reticular body is attached to the coccolith vesicle and is believed to supply matrix material and coccolith constituents for forming coccolith (Corstjens et al., 1998). Within the coccolith vesicle, the microenvironment promotes formation of the coccolith structure and shaping individual crystal units (Henriksen and Stipp, 2009). Newly formed coccoliths consist of 30-40 single crystal calcite units made up of four sub-unit elements. As illustrated in Figure 2, each sub-unit is comprised of a flat 1μm proximal shield element, a hammer-shaped 0.6 μm distal shield element, and a central area element that connects to the proximal and distal shield by an inner tube element. Subunit elements are connected by a vertical extension (Herfort et al., 2004; Young et al., 1992). Once fully formed, the mature coccolith is released from the

cell in a massive exocytoic event when the coccolith vesicle migrates and fuses with the plasma membrane (Henriksen and Stipp., 2009).

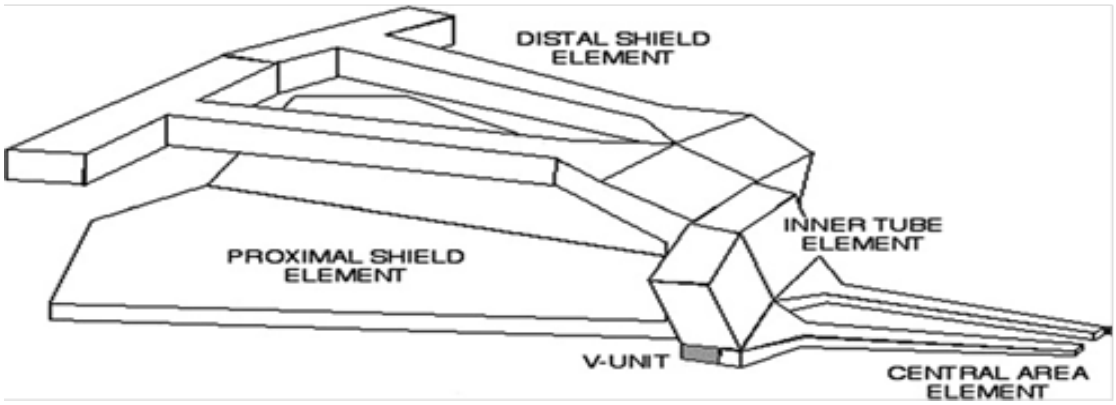

Figure 2: Diagram of *E. huxleyi* coccolith elements. Reproduced from Young et al., (1992).

The coccolith vesicle contains proteins, proteolipids, proteoglycans, and coccolith-associated polysaccharides, some of which might play a role in crystal nucleation and growth (Paasche, 2001). Coccolith polysaccharide is a well characterized macromolecule in *E. huxleyi* coccolith formation. This polysaccharide can inhibit crystallization when it is anchored to the membrane and induce crystal formation and growth when the vesicle becomes dilated (Westbroek et al., 1984). In a study performed by Corstjens and associates (1998), a gene that encodes for proteins glutamic acid, proline and alanine (GPA), was isolated using a cDNA library prepared from *E. huxleyi.* GPA contains high percentages of glutamic acid, proline, and alanine, also harbors a repeat of 12 amino acids that shows homology to the Ca^{2+} binding loop of the typical EF-hand motif. Due to this similarity, GPA was established to be a Ca^{2+} binding protein. GPA has two proposed functions; it may be involved in 1) crystal nucleation and/or regulation of crystal growth or 2) transport of Ca^{2+} from the cell exterior to the coccolith vesicle. Experiments performed by Langer and

colleagues (2010) demonstrated that microfilaments and actin components of the cytoskeleton are involved in coccolith morphogenesis. The study reported an increase in malformed coccoliths when high concentrations of inhibitors colchicine and cytochalasin B were added to *E. huxleyi* cultures. It was found that the inhibitors colchicine and cytochalasin B disrupted microtubules and actin microfilaments respectively and thusly the shaping of coccoliths.

Although the mechanism and function of calcification is not completely understood, several environmental factors including light, temperature, pH, and minerals influence biomineralization in coccolithophorids by affecting coccolith morphology and calcification (Stanley, 2008). Calcification rates are higher in the light as compared to the dark, with little or no calcification occurring at night (Trimborn et al., 2007). When *E. huxleyi* and *G. oceanica* are grown at low temperatures, cells are noticeably larger and feature thick coccospheres, while at high temperatures, cells are smaller with thinner coccospheres (Sorrosa et al., 2005). This suggests that low temperatures induce cell size enlargement while also stimulating coccolith production. *E. huxleyi* cells have a higher growth rate and $CaCO_3$ productivity when grown at an optimal pH of 7.5-8.9 (Moheimani and Borowitzka, 2011; Rhodes et al., 1995). Low calcifying strains prefer a pH of 6.77 ± 0.31 while a high calcifying strains prefer a pH of 7.29 ± 0.11 (Suffrican et al., 2011). Limiting concentration of key minerals, such as calcium and magnesium, lead to malformed coccoliths, under-calcified coccoliths, or no coccolith production (Paasche, 1998; Stanley 2008). When cells are grown in calcium-free or low calcium media, there is a decrease in calcification rates. When cells are grown in high or low magnesium concentrations, coccoliths are typically malformed (Herfort et al., 2004). In contrast, when

cells are grown in high concentrations of sodium bicarbonate, a substrate for calcification, there is an increase in cell diameter, cell volume, and coccolith production (Shiraiwa et al., 2003). Manipulating different concentrations of minerals known to affect coccolith structure such as calcium and sodium bicarbonate may help unveil the fundamental mechanisms that govern calcification in coccolithophores.

Next-generation sequencing

High-throughput quantitative profiling of transcripts and proteins is a powerful method for unraveling the mechanisms governing biological processes. Presently, transcript profiling technologies include DNA microarray, Serial Analysis of Gene Expression (SAGE), and Massive Parallel Signature Sequencing (MPSS) (Hornshol et al., 2009). New technologies have been developed to increase the throughput and reduce the cost of expression profiling. In terms of time, efficiency, cost and the amount of information provided, next-generation sequencing is the most popular method for transcription profiling (Mutz et al., 2013). This technology sequences single DNA fragments, not individual DNA clones, and is based on pyrosequencing, a sequencing-by-synthesis technology (Ansorge, 2009). Next-generation sequencing offers the ability to perform high throughput gene expression profiling, discover non-coding RNA and contribute to genome annotation via short-read sequencing (RNA-seq) (Mutz et al., 2013). RNA-seq is a qualitative transcriptome profiling system that allows for the detection of novel transcripts and the analysis of absolute transcript levels of sequenced and unsequenced organisms.

Currently, 454 genome sequencing FLX (Roche), SOliD (Applied Biosystems) and Solexa/Illumina genome analyzer II are the top sequencing platforms that have transformed and impacted quantitative transcriptomics. These technologies allow for the production of large amounts of data very quickly. Reads are typically 25-450 base- pairs depending on the DNA sequencing technology. Methods can generate data sets up to 50 gigabases per run (Mutz et al., 2013). For example, 454 genome sequencing FLX can generate a reading length of 200-500 nucleotides while Solexa/Illumina and SOliD produce reads of 25-100 nucleotides. In a study by Nagalasksmi and colleagues (2008), RNA-seq technology was used for mapping transcribed regions of the yeast genome. The analyses revealed that 74.5% of the genome's nonrepetitive sequences were transcribed. RNA-seq data allowed the 5' end boundary region of 4665, and the 3' end boundaries of 5215, genes to be defined in yeast. The data also helped to predict uORFs upstream of the start codon for 321 genes (6%) of the yeast transcriptome. RNA-seq technology has also enabled the development of a comprehensive integrated epigenome map for *Arabidopsis thaliana* through direct sequencing of cytosine methylome (methylC-seq), transcriptome (mRNA-seq) and small RNA transcriptome (smRNA-seq). Direct sequencing of the entire cytosine methylome at single-base resolution revealed previously undetected methylation revealing the context and level of methylation at each site. Furthermore, cellular smRNAs deep sequencing unveil a direct relationship between DNA methylation and locations and abundance of smRNAs (Lister et al., 2008).

Using RNA-seq, a transcriptional profiling deep sequencing approach offers the opportunity to study non-model organisms with genomic sequences that are yet to be determined. In a study by Vera and colleagues (2008), 454-based RNA-seq was used to

sequence the transcriptome of the Glanville fritillary butterfly, a nonmodel species. 454 pyrosequencing and *de novo* trancriptome assembly allowed the discovery of: 608,053 expressed sequence tags, 48,354 contigs, 59,943 singletons, and a large number of single nucleotide polymorphisms. The data generated from 454 pyrosequencing can be used to create a microarray for large-scale functional genomics. This technology is not limited to detecting transcripts from model organisms and it can potentially be use for any species (Vera et al., 2008).

The aim of the present research was to use high throughput sequencing RNA-seq methods to compare expression profiles between treatments across the three closely related haptophytes, *E. huxleyi*, *G. oceanica* and *I. galbana*, to discover genes differentially expressed under calcifying and non-calcifying conditions. We attempted to identify potential genes involved in calcification by growing the three sister species under various conditions known to affect biomineralization and comparing transcriptional profiles across species. Cells were grown under calcium rich and calcium deplete conditions, with and without a sodium bicarbonate spike. This research measures physiological parameters for *G. oceanica* including: cell growth, coccolith morphology, rate of calcium uptake and photosynthesis. Previous studies by Schroepfer (2011), measured the physiological parameters for *E. huxleyi* and *I. galbana*. Transcriptome profiles were generated for the three species and a subset of candidate genes expression were validated via real time RT-PCR. By doing this, we tried to identify genes potentially involved in the biomineralization process for the coccolith bearing species *E. huxleyi* and *G. oceanica*. The non-coccolith bearing *I. galbana* was use as a negative control to narrow the list of genes involved in calcification.

Materials and Methods

Cell growth conditions

G. oceanica strain 1281 was purchased from Roscoff Culture Collection (France). Cultures were grown in K/2 media artificial seawater (ASW) (Keller et al., 1987) (400 mM NaCl, 10 mM KCl, 20 mM $MgSO_4 \cdot 7\ H_2O$, 20 mM $MgCl_2 \cdot 6\ H_2O$, 7.5 mM $CaCl_2 \cdot 2\ H_2O$, 0.4 mM HBO_3, 0.88 mM $NaNO_3$, 5µM NH_4Cl, 18µM KH_2PO_4, 5.85 µM FeEDTA), trace elements (76.5 nM $ZnSO_4 \cdot 7\ H_2O$, 39 nM $CuSO_4 \cdot 5\ H_2O$, 910 nM $MnCl_2 \cdot 4\ H_2O$, 26 nM $Na_2MoO_4 \cdot 2\ H_2O$, 11.7 µM $Na_2EDTA \cdot 2\ H_2O$, 0.025µM $CoSO_4 \cdot 7$ H2O, 0.005 µM H_2SeO_3, 0.00314 µM $NiCl_2 \cdot 6H_2O$), and vitamin solution (50 µg/L Biotin, 50 µg/L B_{12}, 100 ng/L thiamine-HCl) at pH 8 as previously described (Guillard, 1975). Cultures were kept at 17-18˚C under cool white fluorescent light (150 µmol m^{-2} S^{-1}) on a 12-hour dark and 12-hour light cycle. The cultures were grown to the late log phase for 7 days with direct cell counts recorded using a hemocytometer and a light microscope on days 2, 4, 6, and 7.

Culture Treatments

E. huxleyi and *G. oceanica,* and the non-calcifying species *I. galbana* cells were grown under conditions known to promote calcification in artificial seawater media with ambient levels of Ca^{2+} (9 mM), and under conditions known to inhibit calcification Ca^{2+} (0 mM). Furthermore, 20 mM sodium bicarbonate, a substrate that affects coccolith formation was added to normal calcium (9 mM) and calcium depleted (0 mM) conditions six days post-inoculation (Table 1). Doubling time calculations were made using the following formula: where t= time in days and q= quantity of cells at time t.

$$T_d = \frac{Log(\frac{q_2}{q_1})}{(t_2 - t_1)Log(2)}$$

Table 1: Concentrations of $Ca^{2+}$and $NaHCO_3$ in the experiments for *E. huxleyi, G. oceanica* and *I. galbana* cells.

Experimental Parameters	Calcium Concentrations	Sodium Bicarbonate Concentrations (6-days post -inoculation)
Condition 1	9 mM	0 mM
Condition 2	9 mM	20 mM
Condition 3	0 mM	0 mM
Condition 4	0 mM	20 mM

Scanning Electron Microscopy

SEM was used to measure growth and the morphology of the coccoliths. For SEM, a volume equivalent to 5.7 x 10^6 cells was filtered onto a polycarbonate (0.8 µM 47 mm) membrane (Millipore #ATTPO4700) and allowed to dry. A total of 8 samples were sent for SEM analysis with 2 images per sample. The filtered membranes were sent to Paul Reidel at PhotoMetrics for SEM imaging.

Calcium Analysis

Complexometric titration with EGTA (ethylene glycol-bis (2-aminoethyl)-tetraacetic acid) is a common method used to directly determine calcium concentration in seawater (Kremling, 1983). The Ca^{2+} concentration was measured by titration according to the protocols of Chisholm and Gattuso (1991). Cell cultures were titrated on day 0, 2, 4, 6, and 7, post-inoculation. The amount of EGTA required to free the GBHA (glyoxal-bis-(2-hydroxanil) of Ca^{2+} is directly proportional to the amount of Ca^{2+} in solution and was used to indirectly estimate rates of calcification.

Calcium Titrations

Post-inoculation, the cells cultured were titrated on days 0, 2, 4, 6, and 7 to determine Ca^{2+} concentrations for each of the treatments. Titrations were performed on three biological replicates. Each replicate contained four samples and each sample was titrated 3 times. Samples were titrated using glyoxal-bis (2-hydroxanil) (GBHA) as a visual metal indicator. When GBHA interacts with the polyvalent cations, calcium, it forms a red chelating agent (complexone). When titrated with EGTA, GBHA is displaced by the EGTA to form a more stable metal complexone. As the concentration of free GBHA in solution increases, color is lost. The amount of EGTA required to displace the red chelating GBHA calcium agent is directly proportional to the Ca^{2+} concentration in the solution. The precision of this method was determined to be better than 0.1% with a coefficient of variation of 0.15% (Kremling, 1983).

To establish the calcium concentration in seawater samples, a standard calcium solution (0.0103M calcium carbonate, 0.3 mM hydrochloric acid, 0.0532 M magnesium nitrate, 0.09 mM strontium chloride, 0.685 M sodium chloride) was prepared and used to standardize the titration (Kremling, 1983). After harvesting cells, the supernatants were titrated. Ten ml of the sample was placed in a beaker, weighed and 95% of the standardized EGTA solution (0.01M) necessary for the endpoint titration was added. The solution was mixed before the addition of 4 ml of 0.05% GBHA (mixed with 1-propanol) and four ml of borax buffer (0.0525 sodium tetraborate; 1.5 M sodium hydroxide) was added to maintain the PH in solution. After stirring for three minutes, the red calcium-GBHA complex formed in solution (Kremling, 1983). Seven ml of 1-butanol was then added to extract the red Ca- GBHA complex into the organic layer. The extraction was immediately

followed by titration using the remaining standardized EGTA solution. The endpoint was indicated by the color change of the organic layer, from red to colorless. The Ca^{2+} content was then calculated with the following equation:

$$\text{mL EGTA} \times \frac{10\ \mu\text{mol EGTA}}{\text{mL EGTA}} \times \frac{1\ \mu\text{mol } Ca^{2+}}{1\ \mu\text{mol EGTA}} = \mu\text{mol } Ca^{2+}$$

Atomic absorption spectroscopy

Atomic absorption spectroscopy is a technique used for the quantitative measurement of chemical elements in solution. This procedure uses the absorption of optical radiation (light) by free atoms in the gaseous state. This technique is based on the fact that metal atoms absorb ultraviolet light when excited by heat. The wavelength absorbed is unique to the particular element. The absorption of light is proportional to the concentration of the element in the sample (Robinson, 1960). In addition to the titration technique described above, atomic absorption was used to measure Ca^{2+} concentrations in solution.

Samples were prepared on day 0, 2, 4, 6 and 7 post -inoculation for each of the four treatment conditions. Samples were centrifuged for 10 minutes at 18 ^{o}C. Then 10 ml of the supernatant of the spent media was filtered using a 0.45 µM filter and a syringe. Samples containing 9 mM calcium were diluted to 5 ppm before filtering. Filtered samples were stored in glass scintillation vials and shipped to Marine Science Institute at the University of California, Santa Barbara for analysis.

Photosynthesis Rates

Photosynthesis rates were estimated by oxygen evolution. This was performed on days 2, 4, 6 and 7 using a Hansatech instrument containing an oxygen electrode system

with OXYGRAPH software (Hansatech,King's Lynn, England). The Oxygraph oxygen electrode control unit measures oxygen via signals from a S1 Clark type electrode disc mounted in a gas-phase oxygen electrode chamber. The Oxygraph oxygen electrode system has been demonstrated to effectively measure oxygen evolution during photosynthesis (Moolna and Rickaby, 2012).

Oxygen evolution was monitored on days 2, 4, 6, and 7 post-inoculation across the four treatments. A total of three biological replicates were measured. Each replicate contained four samples with three oxygen evolution readings per sample. After calibrating the electrode according to the Hansatech instrument manual, a 1 ml of 100X concentrated algal cell sample was placed into the DW1 electrode chamber where oxygen generated from the samples was recorded in nmol/mL. A dual fiber optic light source was used with the fiber placed one inch from the top left side of the chamber delivering 1360 µmol $m^{-2}s^{-1}$ of light to the sample. The oxygen evolution was plotted as an indirect estimate of the rate of photosynthesis (oxygen evolved/unit time). This method is fast and reliable due to the sensitivity of the oxygen electrode.

RNA Extraction

RNA extractions were performed using a traditional guanidium isothiocyante method described by Strommer et al., (1993). RNA was isolated in the late log phase, 7 days post-inoculation, when cell count is at its highest. Coccoliths were dissolved prior to performing extractions as $CaCO_3$ affects both the yield and purity of the RNA. Cells were decalcified by lowering the pH with 0.1M HCl (from pH 8 to pH 5) for two minutes, after which time, the pH was restored to 8.0 with the addition of 0.1 M NaOH. After decalcification, cells were collected and centrifuged (Beckman Coulter Avanti™ J-20 XP

centrifuge) at room temperature, 7500 rpm for 10 minutes. Cells were lysed by grinding in liquid nitrogen using a mortar and pestle and re-suspended in 10 ml extraction buffer. After vortexing for 30 seconds, 1 ml of 2 M sodium acetate (pH 4.0) was added to decrease the pH of the lysate and stabilize the RNA. After vortexing again for 30 seconds, 10 ml of water saturated phenol (pH 4.3) was added to the sample to separate cellular components. The sample was then vortexed for 30 seconds followed by addition of 2 ml of 99.9% chloroform. The sample was then vortexed again for 30 seconds, and centrifuged at room temperature, 5000 g for 10 minutes. This step allowed for separating proteins, lipids and carbohydrates (confined to the organic phase) from the aqueous phase containing the RNA. Upon removing the upper aqueous phase, a second chloroform extraction was performed to minimize DNA contamination. After the second chloroform extraction, an equal volume of cold isopropanol was added to the aqueous phase to precipitate the RNA. The sample was incubated at -20 °C. Following an overnight incubation, RNA was collected by centrifugation at 10,000 g for 10 minutes at 4 °C. The RNA was resuspended in 500 µl RNAse/DNAse-free water and transferred to a 1.5 ml micro-centrifuge tube. An equal amount of 4 M lithium chloride was added to remove remaining contaminants, and the sample was chilled on ice for 1 hour. The RNA sample was centrifuged (Biofuge Fresco Heraeus centrifuge) at 13,000 g for 5 minutes at 4° C and the supernatant was discarded. The RNA pellet was washed with 70% cold ethanol to remove residual lithium chloride. After air-drying for 3-5 minutes, the RNA was resuspended in 30-50 µl of RNAse/DNAse-free water. The purity and concentration of the RNA was determined by using a spectrophotometer, measuring absorbance at 260 nm and 280 nm. The integrity of the RNA was determined by an Experion Automated Electrophoresis system, distributed by Bio-

Rad, which uses lab chip microfluidic technology to automate an electrophoresis for RNA analysis. RNA was then aliquoted and stored in the -80 °C freezer.

Experion RNA Electrophoresis

The Bio-Rad Experion is an automated microfluidic electrophoresis station that combines all electrophoresis steps, including, separation, staining, destaining, band detection, and imaging into a quick 30-minute process. The Experion electrodes were cleaned before and after running the Experion electrophoresis station with the recommended solution and water in the designated “cleaning chips”. Components in the RNA GeneChip kit were allowed to equilibrate at room temperature for 15 minutes, before the gel-stain was prepared by placing 600 µl RNA gel into a filter tube and centrifuging the matrix for 1,500 g for 10 minutes. The filter was discarded and 65 µl of the RNA gel was placed in a new micro centrifuge tube, with 1 µl of RNA stain. The gel-stain was then vortexed and wrapped in aluminum foil to prevent light from degrading the photolabile dye.

The RNA ladder and RNA samples were prepared for chip loading. A total of 1 µl of RNA ladder was used for each chip. Samples were diluted to approximately 100 ng/µl and 2 µl of each sample placed in separate micro centrifuge tubes. The ladder and samples were denatured for 2 minutes at 70°C and then placed on ice.

The Experion RNA StdSens chip was primed with the filtered gel-stain solution by pipetting 9 µl of the gel-stain solution into the gel priming (GS) well and placing the chip in the priming station. After priming the chip, wells were loaded with 9 µl of gel stain, while 9 µl of filtered gel were loaded in the well labeled G. Loading buffer was placed into each of the sample wells. The ladder (1 µl) was loaded into the well labeled L and the

samples were loaded into wells 1-12. Unused sample wells were loaded with 1 µl water when less than 12 samples run.

After loading, the chip was vortexed, placed into the Experion electrophoresis station, and run on the RNA eukaryote setting.

RNA Sequencing

RNA extracted from all four treatment conditions was subjected to transcriptomic analysis using Illumina high-throughput sequencing. Samples were sent to the Beijing Genomics Institute for transcriptome sequencing. Transcripts potentially involved in biomineralization processes were revealed when comparing and contrasting profiles between the three species. The Computational transcriptomic analysis was performed using the de-novo assembler programs Trinity and mapping assembler STAR aligner program (Park, 2013).

To identify potential candidate genes related to biomineralization in the coccolithophorids *E. huxleyi*, *G. oceanica* and *I. galbana* RNA-seq was performed using Illumina high-throughput sequencing technology. The transcriptome for each species was assembled using Trinity which offers two different assembly tools: one of which scaffolds reads against an existing genome sequence and one which builds contigs de-novo using overlapping sequence reads (Park, 2013). The *de-novo* assembled transcriptome of E. *huxleyi* contained 67,797 sequences while that of *G. oceanica* contained 77,634 and that of *I. galbana* contained 47,517 (Appendix A).The expression level of individual genes were then estimated by digital counting reads that aligned to individual transcripts using Bowtie (Park, 2013).

The mapping assembler program was used to assemble reads against existing *E. huxleyi*, *G. oceanica*, and *I. galbana* genome sequences which are estimated to contain 35,582; 52,680; and 18,712 genes, respectively. The mapping assembler matched RNA-seq reads to the reference genomes using STAR aligner and R packages DESeq2 (Hugo et al., 2016). The alignment files were then processed and count matrices of annotated genes in *E. huxleyi*, *G. oceanica* and *I. galbana* were generated. This method successfully mapped 92.5% *E. huxleyi*, 91.7% *G. oceanica* and 94.3% *I. galbana* RNA-seq reads to the draft genomes. The frequency of the reads was statistically analyzed with a negative binomial digital count method (Park, 2013; Anders and Huber, 2010; Werner, 2010). After digitally counting the reads mapping onto the transcriptomes and the genomes, two separate candidate gene lists were generated (Appendix E,F).

Real time RT-PCR

Real time RT-PCR was used to examine expression profiles of a subset of candidate transcripts using RNA extracted from *G. oceanica*. To further validate candidate genes, real time RT-PCR analysis was also performed on total RNA extracted from the *E. huxleyi* non-calcifying (1516) and calcifying (217) strains. First-strand cDNA synthesis was performed using Verso ^{Tm} cDNA kit from Thermo Scientific. For cDNA synthesis, 20 µL reactions were assembled by combining 2 µg of RNA, oligo DT-primer (final concentration 25 ng/µL) and water. After heating samples at 70 °C for 5 minutes to remove secondary structure, 5X cDNA synthesis buffer (final concentration 1X), dNTP mix (500 µM), 1 µL RT enhancer, and 1 µL Verso Enzyme Mix was added to each sample. Finally, samples were mixed and incubated at 42°C for 30 minutes. The RT enzyme was inactivated thereafter by heating to 75 °C for 10 minutes. The final cDNA product was stored in the -

20 °C freezer. For real-time RT-PCR analysis, cDNA was diluted (1:25) and 5 µL of the dilution was used as template.

Real Time RT-PCR was performed according to standard procedures using SYBR green chemistry for amplification detection on an iCycler iQ system (Bio-Rad). Each 25 µL reaction mixture contained 5 µL of diluted cDNA, 12.5 µL of 2X SYBR green master mix (Bio-Rad, Inc), and 0.24 µM of both the forward and reverse primers. Reactions were assembled in a 96-well plate with target as well as housekeeping genes amplified in triplicate as technical replicates. A no template control prepared without cDNA was also prepared and run for each of the different primer sets. A total of three biological replicates were performed for each condition. The cDNA and SYBR green reaction mixtures were loaded into 96-well plates using a Biomeck 2000 Workstation. The plate was then covered with optical seal tape and centrifuged at 500 x g for 1 minute. The thermo-cycling conditions included a 10minute polymerase activation step (95 °C), 40 cycles of denaturing at 95 °C for 10 seconds, annealing at 60 °C for 30 seconds and an extension step at 82 °C for 30 seconds. SYBR green fluorescence was measured at the end of each extension phase. Melt curve analysis was performed after the Real Time RT-PCR amplification whereby products were denatured for 1 minute at 95° C and then cooled for 1 minute at 55° C. The temperature was then increased from 55° C to 95° C in 0.5° C increments every 10 seconds. The data was analyzed using the $2^{-\Delta\Delta CT}$ method to determine the average fold difference in gene expression (Arya et al., 2005; Livak et al., 2001). Two tailed students t-test was used to determine the significance between treatments in a pairwise manner. Primer design parameters, including observed and expected product melting temperatures (Tm), are

found in Appendix B. The overall values for the observed and expected product melting temperatures (Tm) are nearly equivalent to each other.

Results

Cell growth rates for *G. oceanica* growing

G. oceanica, *E. huxleyi* and *I. galbana* cells were grown in artificial sea water in four different calcium conditions. Total cell counts for each individual condition were performed every other day for 7 days as shown in Figure 3. *G. oceanica* cells grown in ASW containing 9 mM of Ca^{2+} were found to have a doubling time of 32.07 ± 5.37 hours (mean ± SD) meanwhile cells grown in 0 mM of Ca^{2+} had a doubling time of 40.18±3.83 hours (mean± SD) during their periods of maximum growth (Table 2).

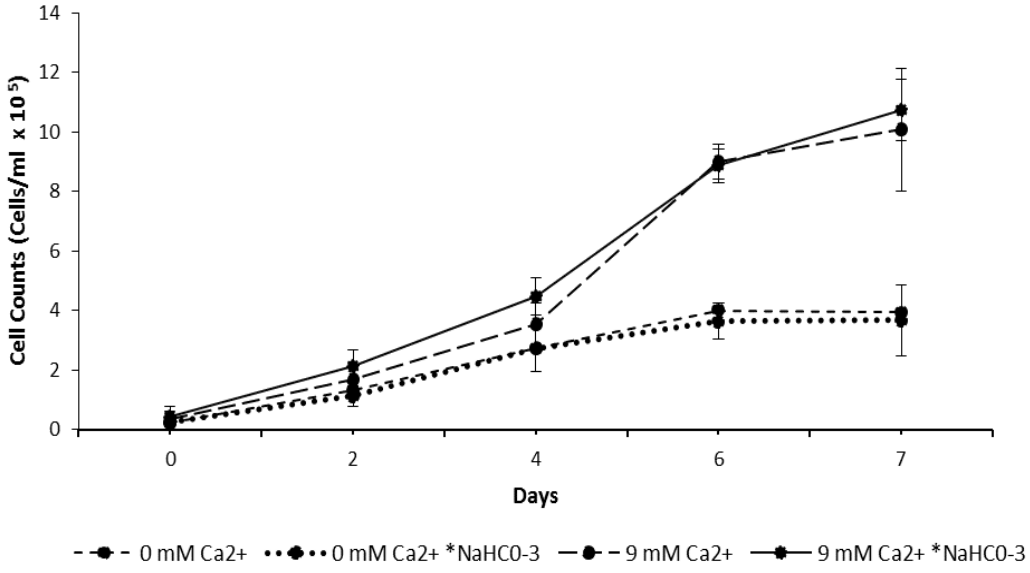

Figure 3: Growth curve for *G. oceanica* in ASW grown in four different conditions.

As shown in table 2**,** *E. huxleyi* cells grown in 9 mM of Ca^{2+} had a doubling time of 23.8 ±0.4 hours (mean ± SD) while cells grown in 0 mM of Ca^{2+} had a slower doubling time of 30.9 ±0.88 hours mean ± SD). *I. galbana* cells grown in 9 mM of Ca^{2+} and in 0 mM of Ca^{2+} showed a slightly longer doubling time of 31.18 ±4.5 hours (mean ± SD) and 36.6 ±7.7 hours (mean ± SD) respectively (Schroepfer, 2011). *G. oceanica* doubling time of 32 hours followed the logarithmic phase growth rate reported by Yamamoto and colleagues, 2000. Meanwhile, *E. huxleyi* growth rate were similar to the 24 hours doubling time reported by Soto et al., 2006. The 31 hours doubling time of *I. galbana* was significantly longer from the 14 hours reported by Gopinathan, 1984.

Table 2: Doubling time for *G. oceanica*, *E. huxleyi* and *I. galbana* during their periods of maximum growth (mean hours± SD).

	Conditions	
Species	9 mM Ca^{2+}	0 mM Ca^{2+}
G. oceanica	32.07 ± 5.37	40.18±3.83
E. huxleyi	23.8 ±0.4	30.9 ±0.88
I. galbana	31.18 ±4.5	36.6 ±7.7

A factorial ANOVA model including all three species *G. oceanica, E. huxleyi* and *I. galbana* had a p-value of 0.30 indicating no significant difference between the doubling times of cells grown in 9 mM of Ca^{2+} and in 0 mM of Ca^{2+} conditions. Furthermore, a two-way ANOVA model between two species for 9 mM of Ca^{2+} and in 0 mM of Ca^{2+} treatments showed no significant difference between *I. galbana* and *E. huxleyi* (p-value=0.10) and *E. huxleyi* and *G. oceanica* (p-value=0.293). Conversely, there is a significance difference between *G. oceanica* and *I. galbana* (p-value < 0.001) cells grown in 9 mM of Ca^{2+} and in 0 mM of Ca^{2+} conditions. In addition, separate 2-tailed t-tests, within *G. oceanica* (p-value

< 0.001) and within *E. huxleyi* (p-value= 0.0303) grown in 9 mM of Ca^{2+} and in 0 mM of Ca^{2+} conditions, indicate significant difference between treatments. However, a 2-tailed t-test for *I. galbana* did not indicate a significant difference (p-value=0.17) between conditions (Schroepfer, 2011).

Coccolith morphology analyzed via scanning electron microscopy

SEM was used to monitor abundance and the morphology of the coccoliths of *G. oceanica* strain 1281 grown in ASW in four different conditions. Cells grown in ASW containing 9 mM of Ca^{2+} displayed well-formed and intact coccoliths (Figure 4 A). In contrast, cells in ASW with 0 mM Ca^{2+} appear to have more malformed and broken coccoliths (Figure 4 B). Cells in ASW containing 9 mM of Ca^{2+} spiked with 20 mM $NaHCO_3$ six days post-inoculation show whole and intact coccolith morphology (Figure 5 A), while, cells in ASW with 0 mM Ca^{2+} spiked with 20 mM of $NaHCO_3$ six days post-inoculation have more broken or malformed coccoliths (Figure 5 B).

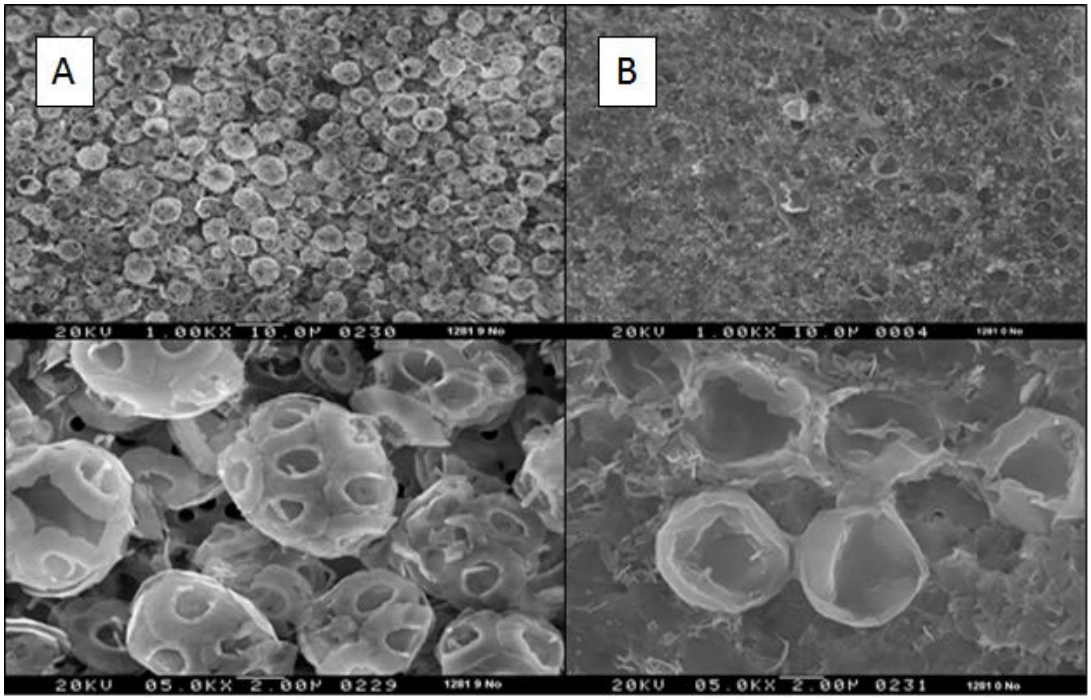

Figure 4: The effect of different calcium concentrations on coccolith structure in *G. oceanica* as depicted by SEM images. Cells were grown in artificial seawater medium containing (A) 9 mM Ca^{2+} and (B) 0 mM Ca^{2+}. Top images at 1000X field, bottom image at 5000X field, 20 kV.

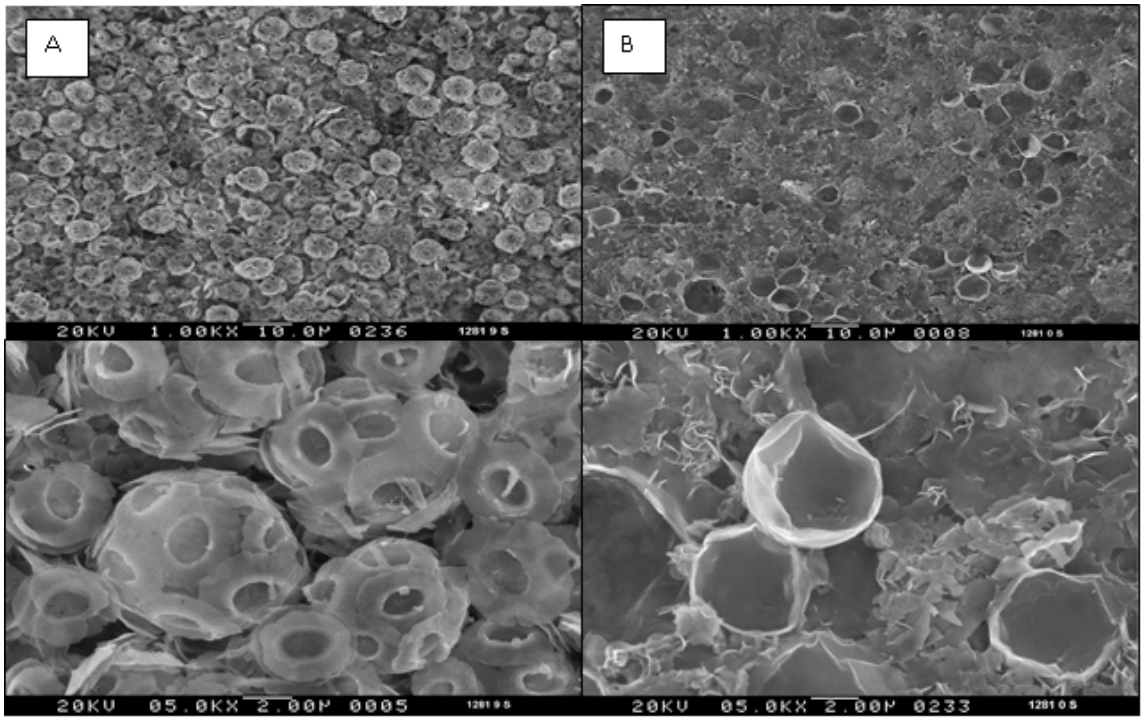

Figure 5: SEM images depicting the effect of different Ca^{2+} and $NaHCO_3$ concentrations in *G. oceanica* cells grown in ASW containing (A) 9 mM of Ca^{2+} spiked with 20 mM $NaHCO_3$ and (B) 0 mM of Ca^{2+} spiked with 20 mM of $NaHCO_3$. Top images at 1000X field, bottom image at 5000X field, 20 kV.

As reported by Schroepfer, 2011, *E. huxleyi* cells grown in 9mM Ca^{2+} and 9 mM of Ca^{2+} spiked with 20 mM $NaHCO_3$ produced whole and intact coccoliths while cells grown in the absence of calcium (0 mM Ca^{2+}, with and without 20 mM $NaHCO_{3-}$ spiked exhibited broken and fragmented coccoliths. Meanwhile, *I. galbana* only showed collapsed cells and no coccoliths were evident under all four growth conditions.

Calcium titration analysis was used to measure calcium in spent media

Calcium titration analysis was used to determine the amount of Ca^{2+} in the spent media of *G. oceanica* cultures grown for 7 days under the four different conditions (Figure 6). A multiway ANOVA model for calcium titration was performed for *G. oceanica* cells grown in 0 mM of Ca^{2+} and 9 mM of Ca^{2+} conditions for 6 days. The model supports that there are significant differences in calcium concentrations between 0 mM of Ca^{2+} and 9 mM of Ca^{2+} conditions ($p < 0.001$) and days 0, 2, 4, 6 ($p < 0.001$). Furthermore, a complex model matrix ANOVA and post-hoc Tukey test performed on R-program indicates a significant difference between days on individual calcium conditions. Significant difference were observed on each individual day: day 0 (p-value < 0.001), day 2 (p-value < 0.001), day 4(p-value =0.002), and day 6 (p-value < 0.001) in the amount of calcium found in the spent media for 9 mM of Ca^{2+} conditions but not under 0 mM calcium condition.

The average amount of calcium found in the media on days 2, 4, 6 and 7 was also determined. Cells grown in 9 mM Ca^{2+} and 9 mM Ca^{2+} spiked with 20 mM $NaHCO_3$ had an average calcium increase of 14.73% between days 0 to day 2 followed by a steady decrease in calcium over the next four days of 3.6 % to 5.8% as shown on figure 6. Meanwhile, cells grown in 0 mM Ca^{2+} and 0 mM Ca^{2+} spiked with 20 mM $NaHCO_3$ had

an average calcium increase of 64.8 % between day 0 to day 2 followed by a variance less than 2% of calcium over the next four days (Figure 6).

The amount of calcium uptake per cell in the spent media was also calculated by dividing the change of calcium per ml per day by the mean number of cells per ml for that day (Figure 7). *G. oceanica* cells grown in 9 mM Ca^{2+} and 9 mM Ca^{2+} spiked with 20 mM $NaHCO_3$ had an overall calcium uptake per cell decrease over time. As shown on figure 7, the average per cell calcium uptake increased per day for days 2 through 6 was 0.00089 pmol Ca^{2+} per cell. For cells grown in 0 mM Ca^{2+} and 0 mM of Ca^{2+} spiked with 20 mM $NaHCO_3$ conditions, between day 2 to day 4 there was a sharp increase of .010 and 0.013 pmol Ca^{2+} respectively per cell followed by a 0.002 pmol Ca^{2+} decrease on day 6 (Figure 7).

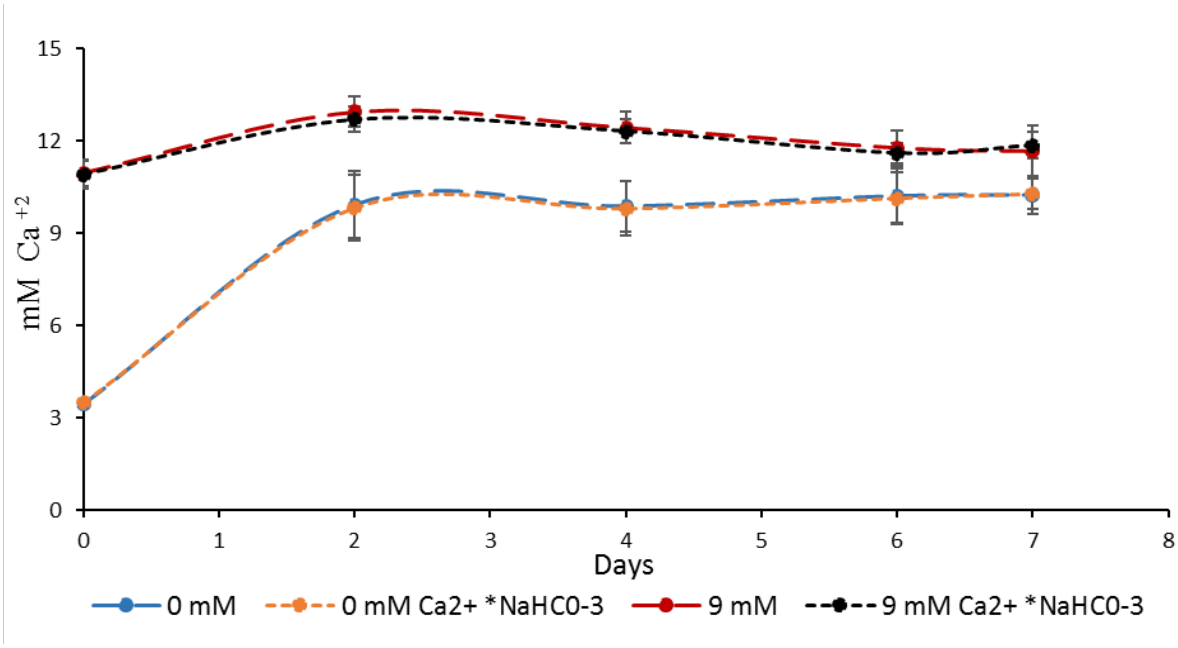

Figure 6: Amount of Ca^{2+} in spent media for *G. oceanica* cells grown in ASW in four different conditions measured utilizing the calcium titration method.

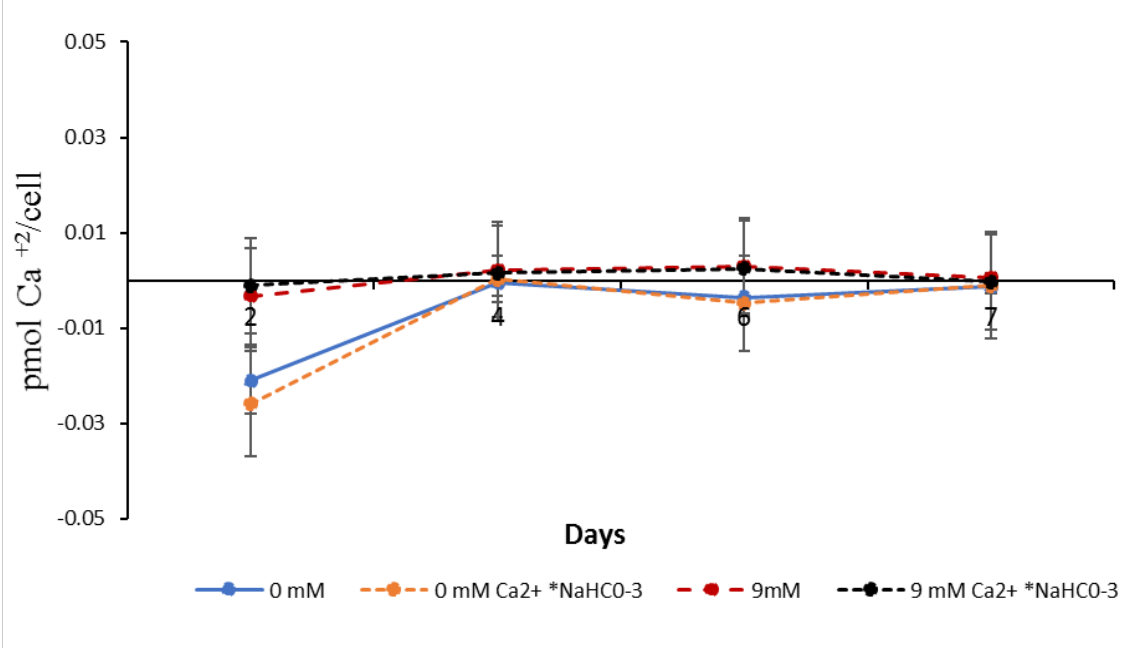

Figure 7: Amount of calcium uptake per cell for *G. oceanica* cells grown in four different conditions using calcium titration analyses.

Furthermore, as reported by Schroepfer, 2011, *E. huxleyi* and *I. galbana* cells grown in 9 mM Ca^{2+} had a 21 µmol and 5 µmol calcium decrease respectively in the spent media from day 2 to day 7. Meanwhile *E. huxleyi* and *I. galbana* cells grown in 0 mM Ca^{2+} had 5 µmol and 12 µmol calcium decrease respectively in the spent media. *E.huxleyi* had a peak calcium uptake per cell on day 2 while *I. galbana* had a decrease calcium uptake per cell followed by a leveling off per cell calcium uptake by day 4 and day 6 for both species.

Calcium in spent media measured by Atomic absorption spectroscopy

Atomic absorption spectroscopy analysis (AAS) was used as an independent means of determining the amount of Ca^{2+} in the spent media of *G. oceanica* cells grown in ASW media under calcium replete and deplete conditions. A multiway ANOVA model for atomic absorption spectroscopy analysis was created for *G. oceanica* cells grown in 0 mM of Ca^{2+} and 9 mM of Ca^{2+} conditions for 6 days. The data shows that there is a significant

difference between the two different calcium conditions 0 mM and 9 mM and the different growth days 0,2,4,6 ($p=0.005$). A post-hoc Tukey test was performed in R-program using an ANOVA complex model matrix script model which indicated a significant difference between individual days: day 0 ($p < 0.001$), day 2($p < 0.001$), day 4($p < 0.001$), day 6 ($p < 0.001$) for 9 mM calcium conditions but not for 0 mm calcium condition. It also supported that there is a significant difference between 9 mM calcium and 0 mM calcium conditions ($P<0.001$).

As evidenced in Figure 8, while calcium in the spent media increased (16.1%) in cells grown in 9 mM Ca^{2+} between day 0 to day 2, there was a steady calcium decrease of 6.6 % for the following four days. On day 7 there was a 27.7% increase for cells grown in 9 mM Ca^{2+} spiked with 20 mM $NaHCO_3$. In contrast, as shown in figure 8, cells grown in 0 mm Ca^{2+} had an average calcium increase of 83.8% between day 0 to day 2 followed by variances of less than 5% of calcium for the next four days. When expressed in terms of calcium per cell in the spent media. *G. oceanica* cells showed fluctuation of calcium uptake for 9 mM Ca^{2+} conditions from day 2 through day 7. As shown in figure 9, calcium uptake per cell for 0 mM Ca^{2+} conditions were relatively constant after day 4. Cells in 9 mM Ca^{2+} had a 70% calcium uptake per cell increase from day 2 to day 4 and a 21% decrease of calcium uptake per cell from day 4 to day 6. In cells grown in 0 mM Ca^{2+} a 38% calcium increase was noted from day 2 to day 4 with a plateau in uptake thereafter (Figure 9).

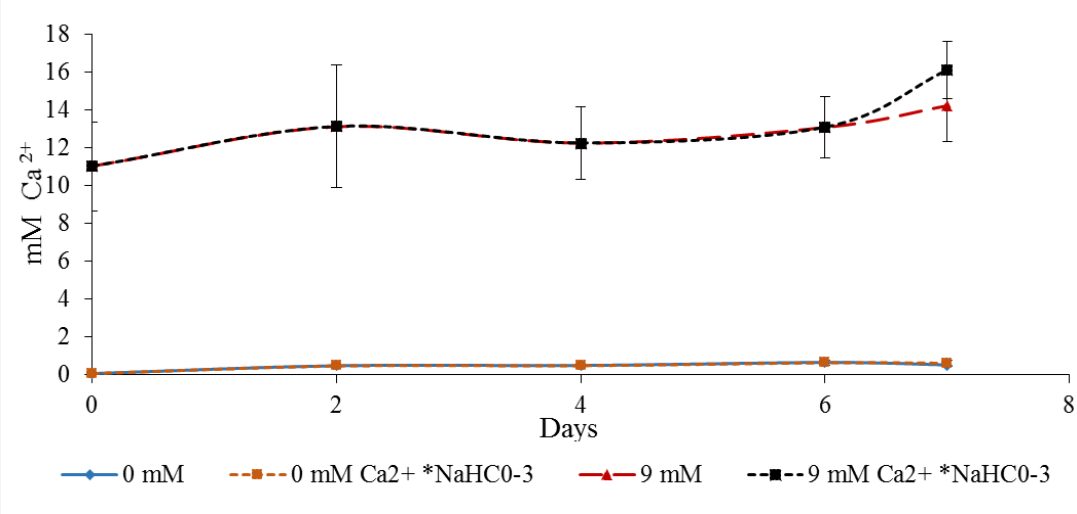

Figure 8: Amount of Ca^{2+} in spent media for *G. oceanica* cells grown in ASW in four conditions using atomic absorption spectroscopy analysis.

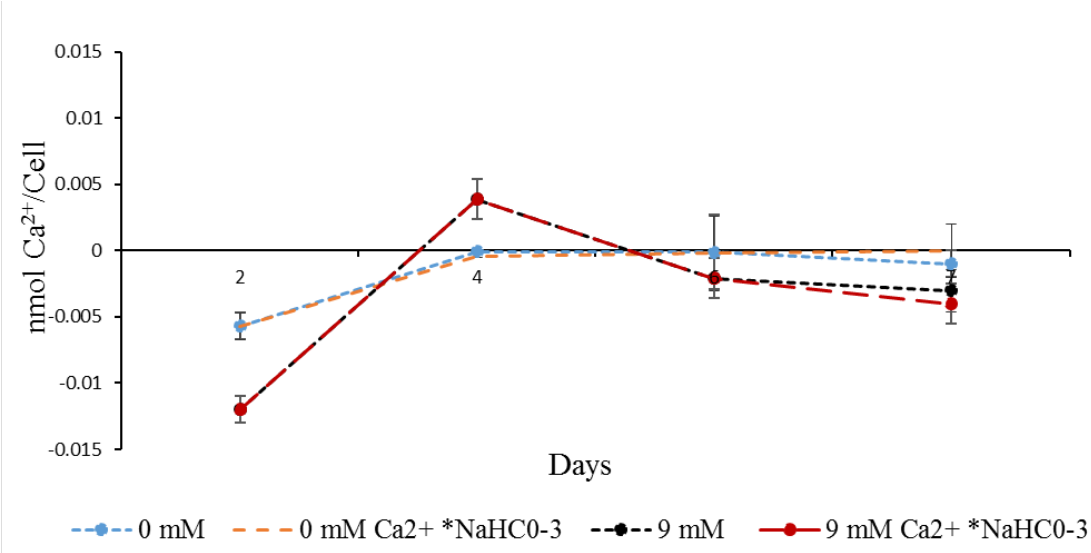

Figure 9: Amount of calcium uptake per cell for G. oceanica cells grown in four different conditions using atomic absorption spectroscopy (AAS) analysis.

Calcium titration and atomic absorption spectroscopy were two methods used to determine the amount of calcium in spent media for *G. oceanica* cells grown in four different conditions for a period of 7 days. Both methods detected differences in the amount of spent media in 0 mM vs 9 mM calcium conditions. Cells grown in 0 mM Ca^{2+} were

shown to have an initial calcium increase from day 0 to day 2 followed by a plateau in uptake in both analyses. Atomic absorption spectroscopy and calcium titration analysis detected calcium increase in the spent media from day 0 to day 6 for cells in 9 mM calcium as seen in Figure 10. Furthermore, a multiway ANOVA was performed for calcium titration and atomic absorption spectroscopy which showed no significance difference ($p = 0.068$) between the two methods.

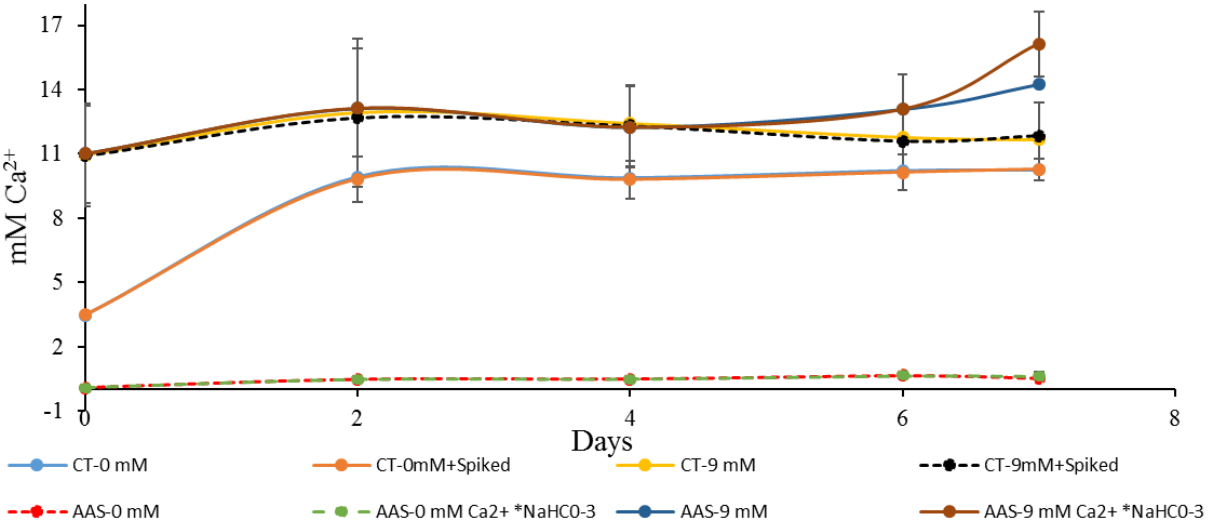

Figure 10: Amount of calcium in spent media in G. oceanica cells using calcium titration (CT) and atomic absorption spectroscopy (AAS) analysis.

Atomic absorption spectroscopy results for the three species:

Atomic absorption spectroscopy was used to detect differences in the amount of calcium in spent media for *E. huxleyi*, *G. oceanica* and *I. galbana* cells grown in 0 mM calcium and 9 mM calcium conditions for a total of 7 days (Figure 11). An ANOVA model test for all three species showed a significant difference between species ($p < 0.001$) and 9 mM and 0 mM calcium conditions($p < 0.001$). A complex model matrix script was performed in the R-program indicating a significant difference for the 9 mM calcium

conditions for day 0 between species *I. galbana* and *E. huxleyi (*$p < 0.001$) and *I. galbana* and *G. oceanica* ($p < 0.004$). On day 2 there is a significant difference between *I. galbana* and *E. huxleyi* ($p < 0.04$) and *I. galbana* and *G. oceanica* ($p < 0.01$). On day 4 there is a significant difference between *I. galbana* and *G. oceanica* ($p < 0.04$). Lastly, on day 6, there is a significant difference between *E. huxleyi* and *G. oceanica* ($p < 0.001$) and *I.galbana* and *E. huxleyi* ($p < 0.001$). There was no significant difference between the three species and the days for 0 mM calcium conditions.

E. huxleyi and *G. oceanica* cells grown in 9 mM Ca^{2+} condition had similar trends for the amount of calcium in the spent media through day 4 as shown in figure 11. Both species had an average calcium increase of 11.6% between day 0 to day 2 followed by continuous calcium decrease less than 5% until day 4. On day 6, *E. huxleyi* had a 12% calcium increase while *G. oceanica* had a less than 1% change. Under 0 mM Ca^{2+} conditions, there was an average 61.3% jump in calcium from day 0 to day 2 followed by a calcium decrease of less than 1% thereafter (Figure 11). The spectroscopy data for *I. galbana* cells grown in 9 mM Ca^{2+} shows a trend of continual calcium increase in the media of less than 1% from day 0 through day 6. Under 0 mM Ca^{2+} conditions, there is a rise of 84.1 % of calcium between day 0 to day 2 followed by an incremental increase of less than 1% from day 2 through day 6 (Figure 11).

The amount of calcium uptake per cell was determined for *E. huxleyi, G. oceanica* and *I. galbana* cell grown in 0 mM Ca^{2+} and 9 mM Ca^{2+} conditions by assuming any increase or decrease in the calcium of the media is a flow of calcium into and out of the cells. As shown in figure 12, *E. huxleyi,* and *G. oceanica* in 9 mM Ca^{2+} had an initial 18.4%

and 18.0% decrease in per cell calcium uptake respectively on day 2 resulting in a increase in the amount of calcium found in the media. On day 4, there was an average 20.0% increase in calcium uptake followed by an average 6% decrease of calcium on day 6 (Figure 12). Conversely, *I. galbana* had an initial 5% increase in calcium uptake per cell on day 2 followed by a 4% decrease of calcium thereafter. For cells grown in 0 mM calcium, there was an average 66.1% decrease in calcium uptake on day 2 followed by an average calcium uptake of 5% for the remaining four days for all three species (Figure 12). The overall trend for cells grown in 9 mM calcium conditions showed fluctuation in the amount of calcium uptake per cell over time, while there is very little variation for cells grown in 0 mM calcium conditions.

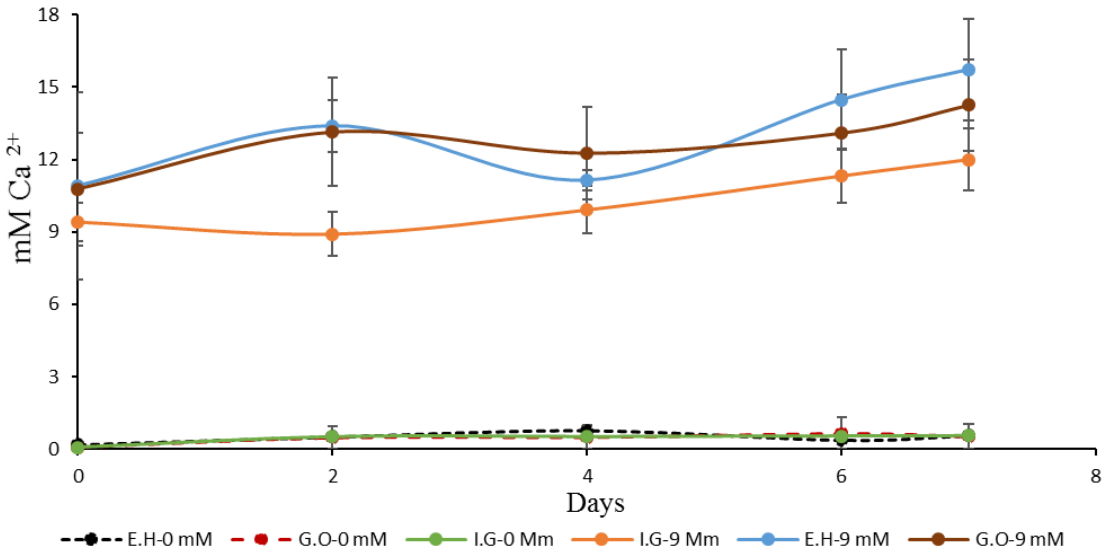

Figure 10: Amount of calcium in spent media for *E. huxleyi*, *G. oceanica*, and *I. galbana* cells grown in ASW in 0 mM Ca^{2+} and 9 mM Ca^{2+} conditions using atomic absorption spectroscopy.

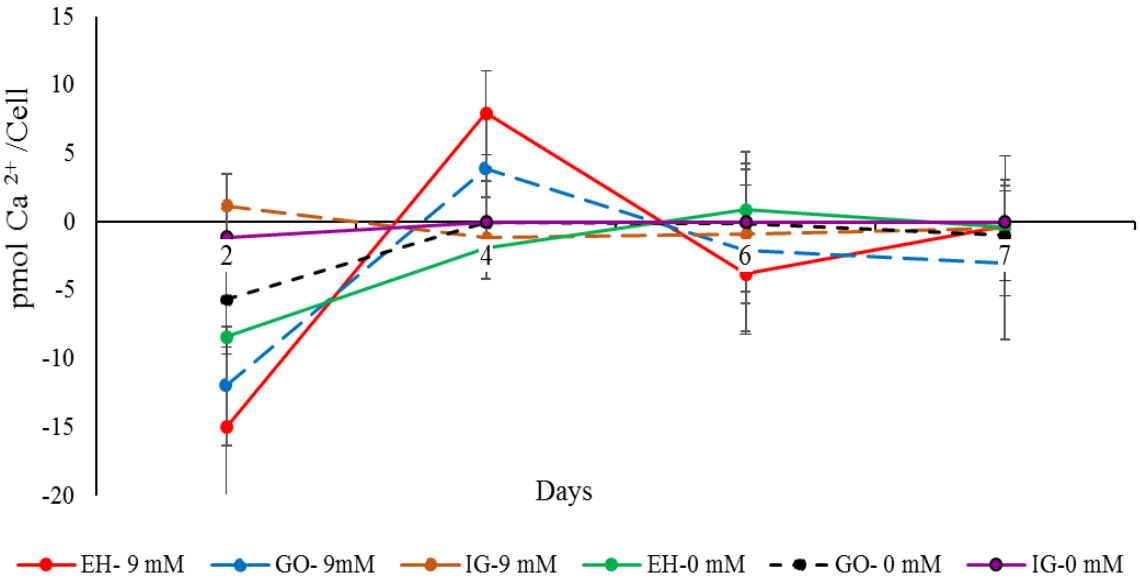

Figure 11: Amount of calcium uptake per cell for *E. huxleyi*, *G. oceanica* and *I. galbana* cells grown in 0 mM Ca^{2+} and 9 mM Ca^{2+} conditions using atomic absorption spectroscopy analysis

Oxygen evolution as an indirect measurement for photosynthesis rates

Gross photosynthesis rates were monitored over a period of 7 days for *G. oceanica* cells grown in 9 mM Ca^{2+} and 0 mM Ca^{2+} with and without a 20 mM of $NaHCO_3$ spike by measuring the O_2 evolution/production (Figure 13). A multiway ANOVA was performed for photosynthesis rates and it showed a significant difference between 9 mM and 0 mM conditions ($p < 0.001$) and significance difference between days 2, 4, 6 ($p < 0.001$) for individual conditions. Furthermore a 2-tailed t-test ($p<0.001$) indicates significant differences between 9 mM and 0 mM calcium conditions. As shown in figure 13, cells grown in media containing 9 mM Ca^{2+} had a continuous photosynthesis rate increase of 57.7% and 25.9% from day 2 to day 6. Meanwhile, cells grown in 0 mM Ca^{2+} had a continuous photosynthesis rate increase of 15% to 8% from day 2 to day 6. On day 7 cell

grown in 9 mM calcium conditions have a rate decline of 23.7 % while cells in 0 mM calcium have showed a 20 % photosynthesis rate increase.

Photosynthesis rates per cell were measured by dividing the amount of O_2 by the number of cell per ml for that day. A 2 tail-t-test was performed and found significant difference (P=0.03) in photosynthesis rates per cell for 9 mM and 0 mM calcium conditions. As shown in figure 14, cells grown in 9 mM Ca^{2+} showed a 37.7% decrease in photosynthesis rates per cell from day 2 to day 4 followed by a decrease of 24.5% thereafter Furthermore, cells grown in 0 mM Ca^{2+} had a continuous decline per cell photosynthesis rates of 18.3% between day 2 to day 4 followed by a 7.1 % for day 4 to day 6. On day 7, there is a rise of 11.9 % for cells grown in 0 mM Ca^{2+} spiked with 20 mM of $NaHCO_3$ (figure 14).

Meanwhile, as reported by Schroepfer, 2011, photosynthesis rates for both *E. huxleyi* and *I. galbana* grown 9 mM Ca^{2+} and 0 mM Ca^{2+} followed similar trends regardless of species. Both species had higher photosynthesis rates for cells grown in 9 mM Ca^{2+} and a constant per cell rate for both calcium conditions.

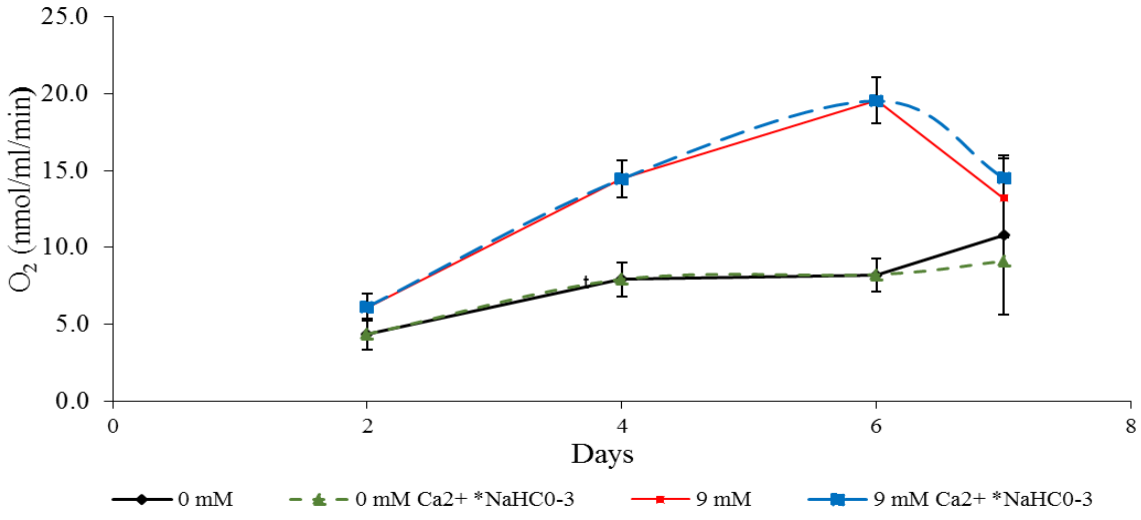

Figure 12: O_2 evolution was used to measured photosynthesis rates for *G. oceanica* grown in four different conditions.

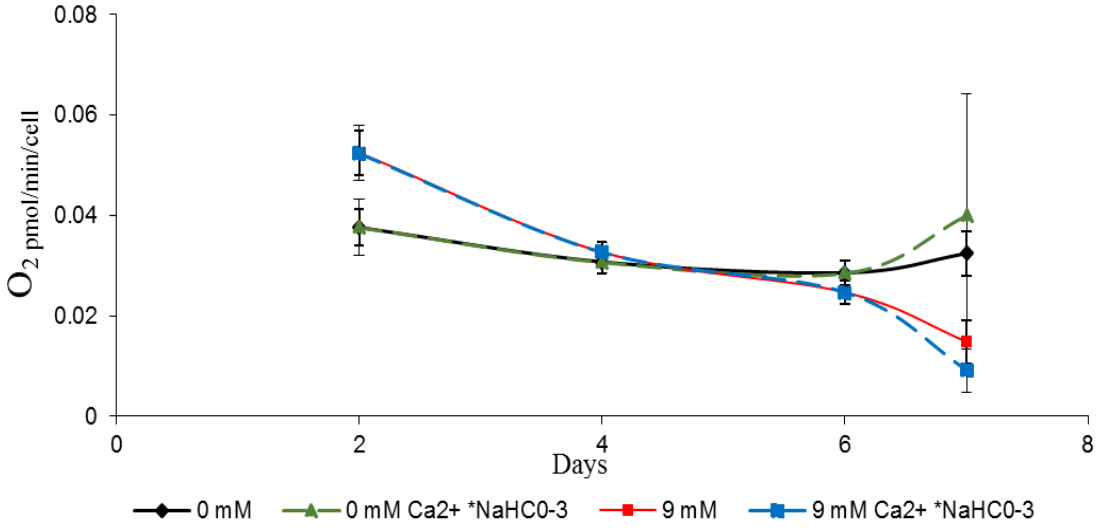

Figure 13: Oxygen production per cell determined by O_2 evolution over time for *G. oceanica* grown in four different conditions.

RNA Extraction and Experion RNA Electrophoresis assessing RNA quality

RNA was extracted from *E. huxleyi*, *G. oceanica* and *I. galbana* cells grown under the different calcium conditions. Total RNA extracted was used for

Solexa/Illumina high-throughput sequencing profiles. Over 100 sets of independent RNA extractions with four samples per set were performed for the three species. Sets of 3 biological replicates with four samples per set for a total of 36 independent RNA extractions for all three species were sent to Beijing Genomics for transcriptome sequencing. The remaining extracted RNA for *E. huxleyi* and *G. oceanica* was used for real time RT-PCR analysis. The quality of the sent RNA was determined via concentration and purity of the sample. The RNA samples had concentrations that ranged from 1623.1 ng/µl to 3564.1 ng/µl, with an average value of 2569.1 +/- 662.0. The purity of the samples for the 260/280 ratios had a range of 1.81 to 2.1 (Table 3), with the average being 1.99 +/- 0.095.

Integrity of the RNA was confirmed using a Bio-Rad Experion ® microfluidic chip. The Experion ™ software produces a virtual gel image to generate RNA bands corresponding to the 28S and 18S ribosomal RNA subunits. The Experion ™ system also quantifies the 28S to18S rRNA ratio. High integrity samples exhibit 28S:18S rRNA ratios close to 2. An RNA quality Index (RQI) score on a scale of 1 to 10 is also computed for each sample, whereby 1 indicates totally degraded sample and 10 intact high quality RNA (Bio-Rad tech note 5761). The integrity of the RNA extracted for *E. huxleyi, G. oceanica* and *I. galbana* cells under the four different conditions was mostly intact with a RQI score ranging from 8.0 to 9.8, with an average of 9.01, and 28S and 18S rRNA ratios ranging from 1.16 to 2, with an average of 1.66 (Figure 15).

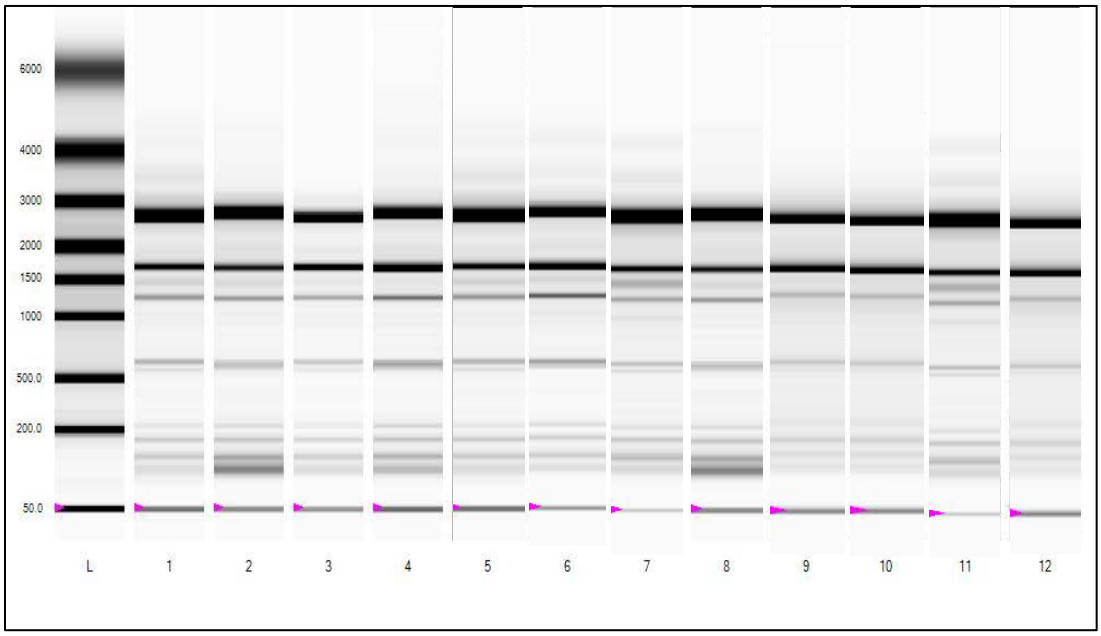

Figure 14: Experion TM gel image from RNA chip for RNA extracts. The 1st lane had the ladder(L) while lanes 1-4 contain *E. huxleyi*, lanes 5-8 had *G. oceanica* and lanes 8-12 contained I. galbana samples corresponding to 9 mMCa^{2+}, 9 mM Ca^{2+} + 20 mM $NaHCO_3$, 0 mM Ca^{2+} and 0 mM Ca^{2+} + 20 mM $NaHCO_3$ respectively.

Table 3: Concentration and purity for cells grown in four different calcium conditions. Quality analysis included RNA quality, purity and RQI (RNA quality index) for *E. huxleyi*, *G. oceanica* and *I. galbana*.

Sample	Treatment	Nanodrop			Experion™	
		Ng/µL	260/280	260/230	28s:18s	RQI
E.hux -1	9 mM	2065.2	2.09	2.20	1.46	9.1
E.hux -1	9 mM + $NaHCO_3$-	2012.0	1.84	1.96	1.54	9.1
E.hux -1	0 mMol	2077.3	2.12	2.23	1.71	8.9
E.hux- 1	0 mMol + $NaHCO_3$-	2313.0	2.08	2.09	1.56	8.7
E.hux -2	9 mMol	1699.3	2.06	2.01	1.46	8.0
E.hux -2	9 mMol + $NaHCO_3$-	3534.7	2.00	2.07	1.67	9.6
E.hux -2	0 mMol	2817.4	2.05	2.04	1.57	8.9
E.hux -2	0 mMol + $NaHCO_3$-	1747.0	2.05	1.85	1.47	9.5
E.hux -3	9 mMol	2992.3	2.02	1.98	1.62	8.1
E.hux -3	9 mMol + $NaHCO_3$-	2258.2	2.04	1.83	1.66	8.3
E.hux -3	0 mMol	2693.8	2.04	2.02	1.78	8.4
E.hux -3	0 mMol + $NaHCO_3$-	3389.0	2.05	2.08	2.00	9.8
G.O -1	9 mMol	2927.2	2.05	1.90	1.62	9.0
G.0 -1	9 mMol + $NaHCO_3$-	2710.4	1.82	1.89	1.58	8.4
G.0 -1	0 mMol	1926.8	2.07	2.05	1.58	8.9
G.O -1	0 mMol + $NaHCO_3$-	2009.4	2.08	1.99	1.63	8.5
G.0 -2	9 mMol	3234.9	2.04	2.08	1.16	8.8
G.0 -2	9 mMol + $NaHCO_3$-	2913.1	1.85	1.87	1.43	9.2
G.0 -2	0 mMol	1623.1	2.12	1.99	2.00	9.0
G.0 -2	0 mMol + $NaHCO_3$-	1655.4	2.13	2.09	2.00	8.4
G.0 -3	9 mMol	2292.1	2.06	1.96	1.77	8.5
G.0 -3	9 mMol + $NaHCO_3$-	2532.8	1.94	1.90	1.81	8.7
G.0 -3	0 mMol	1680.7	2.07	1.92	2.00	9.0
G.0 -3	0 mMol + $NaHCO_3$-	1630.0	1.91	1.88	1.57	8.7
I.G -1	9 mMol	2670.3	2.01	1.86	1.60	9.2
I.G -1	9 mMol + $NaHCO_3$-	2346.5	2.06	2.04	1.75	9.4
I.G -1	0 mMol	1613.6	2.06	1.98	1.73	9.5
I.G -1	0 mMol + $NaHCO_3$-	3235.6	1.81	1.95	1.48	9.6
I.G -2	9 mMol	3390.5	1.92	2.00	1.76	9.5
I.G -2	9 mMol + $NaHCO_3$-	3377.7	1.98	1.94	1.54	9.3
I.G -2	0 mMol	2288.6	2.02	1.90	1.61	9.1
I.G -2	0 mMol + $NaHCO_3$-	3033.1	1.85	1.97	1.76	9.6
I.G -3	9 mMol	3498.0	1.88	1.94	1.65	9.8
I.G -3	9 mMol + $NaHCO_3$-	3466.8	1.86	1.87	1.53	8.6
I.G -3	0 mMol	3564.1	1.92	1.98	1.78	9.8
I.G -3	0 mMol + $NaHCO_3$-	3267.0	1.89	2.00	1.97	9.7

RNA Sequencing used for comparative transcriptomics

The first RNA-seq gene list, Geph_DE0V9_padj0.1_in-ehux-not-iso, was generated using mapping assembler STAR and DEseq2 mapping tools and is based on digital counts to the sequenced genomes. The list contains 295 differentially expressed genes found in *E. huxleyi* and *G. oceanica* but not in *I. galbana* when comparing calcium replete and deplete conditions. From this list, a set of 11 genes (the top 5 most up-regulated and the 6 most down-regulated) were chosen for real time RT-PCR based on p-value (Table 4). The second RNA- seq gene list blast2go-table_20141106_1156, was produced using digital counts when reads were mapped to the individual transcriptomes and contained 44 differently expressed genes and isoforms found in *E. huxleyi* when comparing across the same calcium replete and deplete conditions. From this list, a set of 10 genes considered the most statistically significant differentially expressed genes were selected for independent real time RT-PCR validation (Table 5). Some of the genes on the list of candidates likely to be involved in biomineralization included transcripts showing significant homology to zinc iron permeases, protein kinase, and aspartyl beta-hydroxylase (Table 4, 5).

Table 4: The 11 most differentially expressed genes in 9 mM Ca^{2+}conditions found in *E. huxleyi* and *G. oceanica* but not in *I. galbana* when comparing cultures grown in calcium replete versus deplete conditions. Sequence name, protein identification, hit description, and p-value were taken from RNA-seq data list Geph_DE0V9_padj0.1_in-ehux-not-iso generated by mapping reads to the genome.

List name: Geph_DE0v9_padj0.1_in-ehux-not-iso

Up-Regulated in Calcification Promoting Conditions

Sequence Name	**Protein ID**	**Hit Description**	**P-value**
evm.model.Contig1153.18	103255	Chaperone protein	2.52E-08
evm.model.Contig1521.3	199016	Translation initiation Factor IF-2	6.44E-10
evm.model.Contig1110.19	353012	Zinc/ iron permease	1.16E-14
evm.model.scaffold_309.27	240483	Zinc/ iron permease	1.04E-07
evm.model.scaffold_105.33	222767	Rtx toxin/ATPase binding	2.92E-05
Down- Regulated in Calcification Promoting Conditions			
evm.model.scaffold_282.3	46343	Membrane protein	7.12E-10
evm.model.scaffold_161.21	432991	Membrane Protein	1.61E-05
evm.model.Contig1564.12	230169	Protein Kinase domain	3.58E-09
evm.model.Contig909.12	100838	Hypothetical protein	3.01E-06
evm.model.Contig874.8	215610	Hypothetical protein	1.45E-07
evm.model.Contig92.21	107263	Hypothetical protein	2.33E-08

Table 5: The10 most statistically significant differentially expressed genes in 9 mMCa^{2+} found *E. huxleyi* and *G. oceanica* but not in *I. galbana* when comparing cultures grown in calcium replete versus deplete conditions. Sequence name, protein identification, hit description, and E-value were taken from RNA-seq. data list blast2go-table_20141106_1156 generated by mapping reads to the transcriptome.

Up-Regulated in Calcification Promoting Conditions			
Sequence Name	**Protein ID**	**Hit Description**	**E-value**
c31156_g1_i13	558392	Type I phosphodiesterase nucleotide pyrophosphatase	1.39E-144
c30483_g7_i1	218042	Two component response regulator	9.63E-76
c30989_g4_i2	199868	Myosin VI/myosin complex	1.38E-147
c27445_g3_i9	464892	Hemolysin-related protein	2.31E-40
c5364_g1_i1	447372	Endo- -beta-xylanase	4.56E-95
c22401_g2_i1	46378	Vomi family protein	1.86E-84
Down -Regulated in Calcification Promoting Conditions			
c13659_g2_i1	365512	Predicted uncharacterized protein LOC104115559	1.76E-09
c28658_g1_i4	210744	Clavaminates synthase	0
c27886_g1_i2	450163	Aspartyl beta-hydroxylase / Beta- aspartyl asparaginyl family	0
c31037_g3_i14	211953	Endoplasmic reticulum mannosyl-oligosaccharide -alpha-mannosidase-like isoform x1	0

Real-Time RT- PCR validation for *G. oceanica*

Real time RT-PCR for *G. oceanica* was used to independently validate differential expression for 5 of the 11 genes generated by mapping reads to the genome (45%) (Table 6). The expression levels for membrane protein and hypothetical proteins were an average of 4- fold higher under calcium limiting versus calcium replete conditions. The expression level of a putative chaperone protein and a translation initiative Factor IF-2 protein, on the other hand, were nearly 10- fold higher when cells were grown under ambient calcium versus limiting calcium (Figure 16).

Table 6: The relative expression pattern between RNA-seq list Geph_DE0V9_padj0.1_in-ehux-not-iso generated by mapping reads to the genome and real time RT-PCR analysis using *G. oceanica* RNA.

Sequence Name	Protein ID	Hit- Description	RNA-Seq.	*G.O*-PCR
evm.model.Contig1153.18	103255	Chaperone protein	Down	Down
evm.model.Contig1521.3	199016	Translation initiation Factor IF-2	Down	Down
evm.model.Contig1110.19	353012	Zinc iron permease	Down	UP
evm.model.scaffold_309.27	240483	Zinc iron permease	Down	UP
evm.model.scaffold_105.33	222767	Rtx toxin/ATPase binding	Down	UP
evm.model.scaffold_282.3	46343	Membrane protein	UP	UP
evm.model.scaffold_161.21	432991	Membrane Protein	UP	Down
evm.model.Contig1564.12	230169	Protein Kinase domain	UP	Down
evm.model.Contig909.12	100838	Hypothetical protein	UP	UP
evm.model.Contig874.8	215610	Hypothetical protein	UP	UP
evm.model.Contig92.21	107263	Hypothetical protein	UP	Down

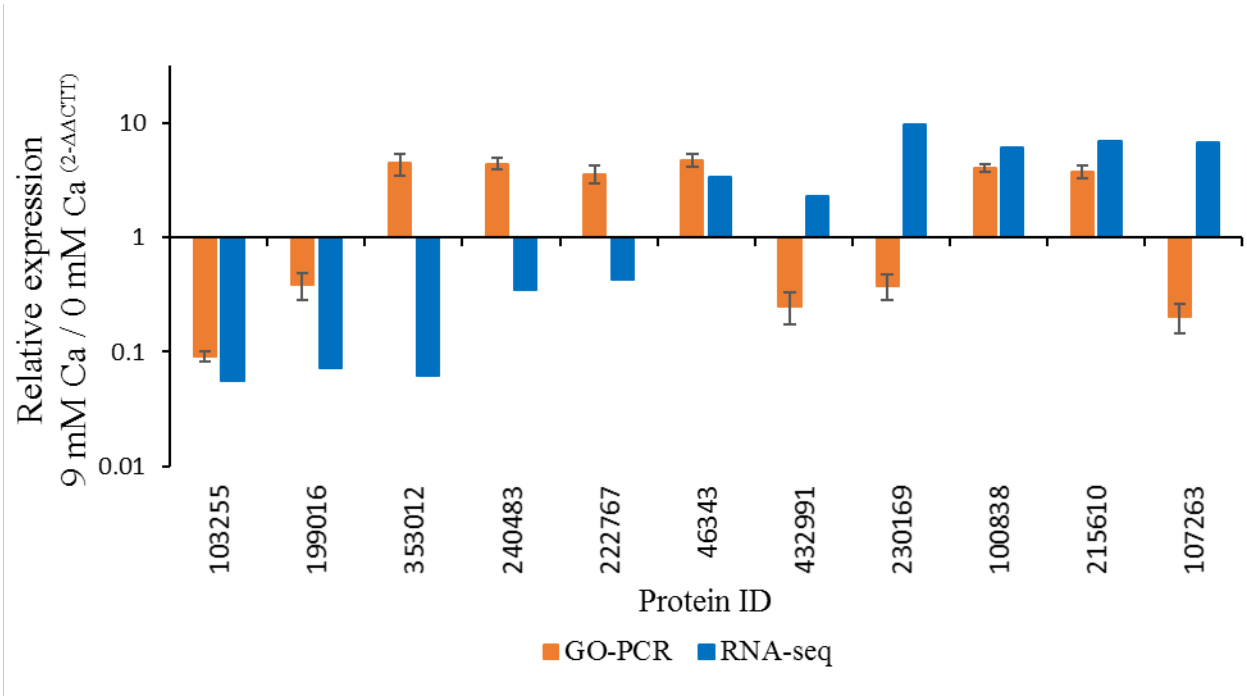

Figure 15: Comparison between *G. oceanica* real-Time RT-PCR gene expression level and RNA-seq. list Geph_DE0V9_padj0.1_in-ehux-not-iso data generated by mapping reads to the genome of 9 mM Ca^{2+} relative to 0 mM Ca^{2+}.

Real Time RT-PCR validation for *E. huxleyi* 217

When independently validating the expression of genes in *E. huxleyi* strain 21, only 6 of the 11 genes (54%) showed concordant results when comparing RNA-seq. data generated by mapping reads to the genome and real time RT-PCR data (Table 7). Real time RT-PCR identified a difference in expression levels for 6/6 genes that were considered upregulated (100%). Of the 6 transcripts tested for expression levels, membrane protein 46343 was found to be the most significantly differently expressed. This membrane protein was up-regulated 17fold when cells were grown in 9 mM Ca^{2+} compared to 0 mM Ca^{2+} (Figure 17). A number of hypothetical proteins (432991, 230169, 100838, 215610, and 107263) and a putative protein kinase are amongst the significantly differently expressed transcripts that according to the real time RT -PCR data had an average fold change of 3-9 when calcium was limiting.

Table 7: The relative gene expression pattern between RNA-seq list Geph_DE0V9_padj0.1_in-ehux-not-iso generated by mapping reads to the genome and real time RT-PCR analysis using *E. huxleyi* 217 RNA.

Sequence Name	**Protein ID**	**Hit- Description**	**RNA-Seq.**	***E.H-217*-PCR**
evm.model.Contig1153.18	103255	Chaperone protein	Down	UP
evm.model.Contig1521.3	199016	Translation initiation Factor IF-2	Down	UP
evm.model.Contig1110.19	353012	Zinc iron permease	Down	UP
evm.model.scaffold_309.27	240483	Zinc iron permease	Down	UP
evm.model.scaffold_105.33	222767	Rtx toxin/ATPase binding	Down	UP
evm.model.scaffold_282.3	46343	Membrane protein	UP	UP
evm.model.scaffold_161.21	432991	Membrane Protein	UP	UP
evm.model.Contig1564.12	230169	Protein Kinase domain	UP	UP
evm.model.Contig909.12	100838	Hypothetical protein	UP	UP
evm.model.Contig874.8	215610	Hypothetical protein	UP	UP
evm.model.Contig92.21	107263	Hypothetical protein	UP	UP

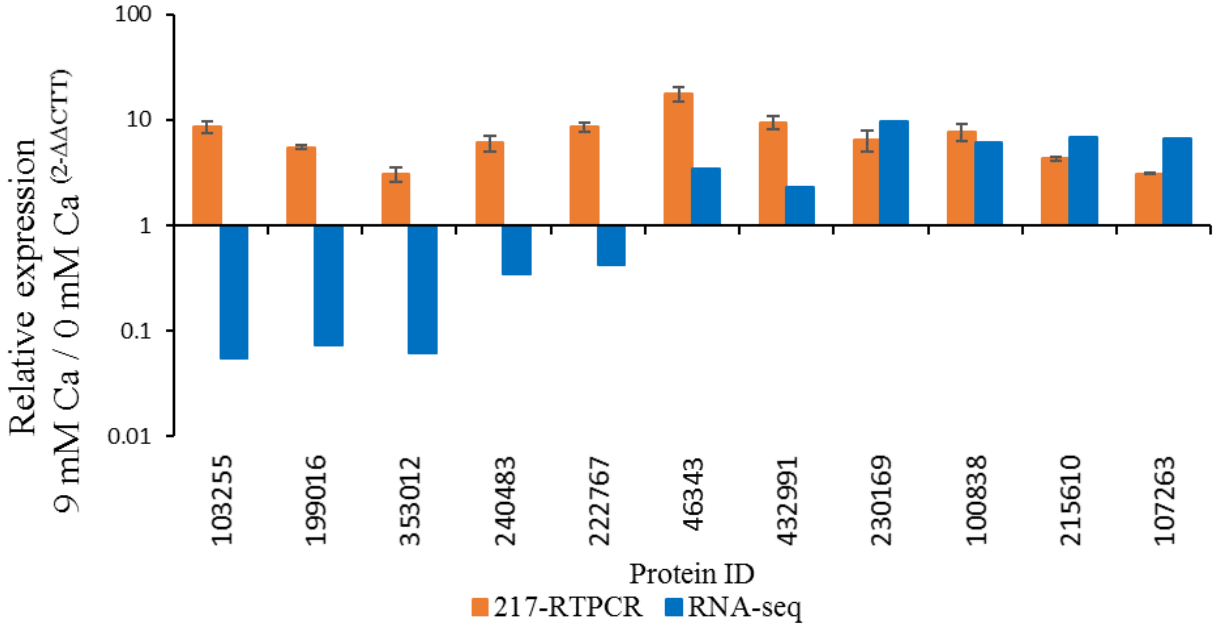

Figure 16: Comparison between *E. huxleyi* (217) Real-Time RT-PCR gene expression levels and Rna-seq. Geph_DE0V9_padj0.1_in-ehux-not-iso. data generated by mapping reads to the genome of 9 mM Ca^{2+} relative to 0 mM Ca^{2+}.

Real Time RT-PCR validation for *E. huxleyi* 1516

To further validate candidate genes involved in biomineralization, real time RT-PCR was performed on *E. huxleyi* non-calcifying strain (1516) and a calcifying *strain (*217). *E. huxleyi* 1516 real time RT-PCR data was only able to validate 4 of the 11 genes (36%) of the differentially expressed genes when compared to the RNA-seq data generated by mapping reads to the genome. The data identified a difference in expression for 2/6 genes that were considered up-regulated (33%) and 2/5 genes were considered down regulated (40%) compared to the RNA-seq. data (Table 8). The two transcripts with the highest expression levels were membrane protein 46343 and hypothetical protein (107263). Membrane protein 46343 was up-regulated and it had a 3fold increase while hypothetical protein 107263 had a 2 fold increase when cells were grown in 9 mM Ca^{2+}

and 0 mM Ca^{2+}conditions (Figure 18). These results were consistent with data from *E. huxleyi* 217 real time RT-PCR. The similarities between calcifying (217) and non-calcifying (1516) strains for membrane protein (46343) and hypothetical protein (107263) were unexpected. Strain 1516 does not calcify and presumably does not express the necessary biomineralization transcripts.

Table 8: Real time RT-PCR relative gene expression pattern for a) *E. huxleyi* 217 vs b) 1516 and Rna-seq. list Geph_DE0V9_padj0.1_in-ehux-not-iso data generated by mapping reads to the genome.

Sequence Name	**Protein ID**	**Hit- Description**	**RNA-Seq.**	***E.H-217*[a]**	***E.H-1516*[b]**
evm.model.Contig1153.18	103255	Chaperone protein	Down	UP	UP
evm.model.Contig1521.3	199016	Translation initiation Factor IF-2	Down	UP	UP
evm.model.Contig1110.19	353012	Zinc iron permease	Down	UP	Down
evm.model.scaffold_309.27	240483	Zinc iron permease	Down	UP	Down
evm.model.scaffold_105.33	222767	Rtx toxin/ATPase binding	Down	UP	UP
evm.model.scaffold_282.3	46343	Membrane protein	UP	UP	UP
evm.model.scaffold_161.21	432991	Membrane Protein	UP	UP	Down
evm.model.Contig1564.12	230169	Protein Kinase domain	UP	UP	Down
evm.model.Contig909.12	100838	Hypothetical protein	UP	UP	Down
evm.model.Contig874.8	215610	Hypothetical protein	UP	UP	Down
evm.model.Contig92.21	107263	Hypothetical protein	UP	UP	UP

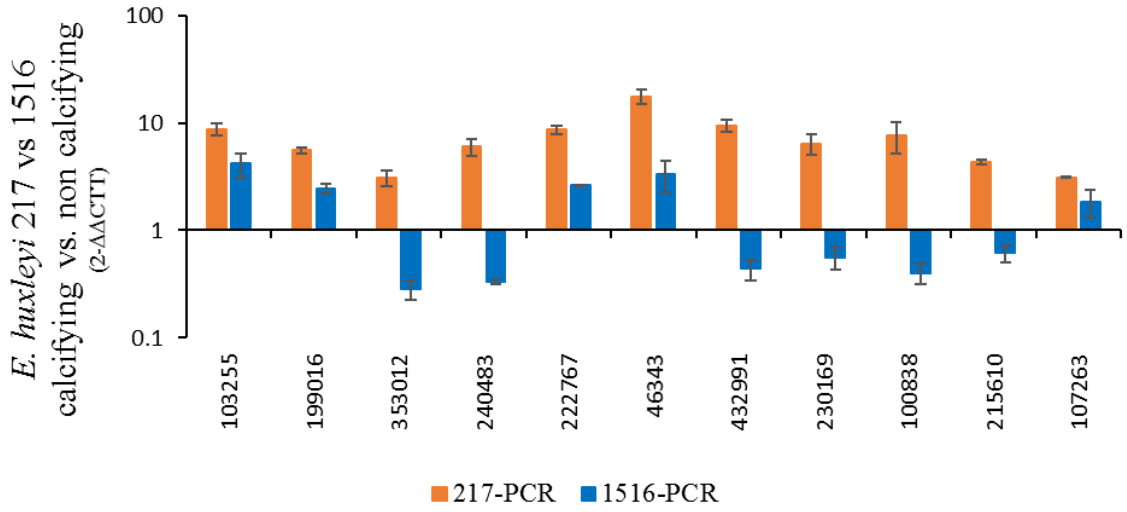

Figure 17: Real time RT-PCR relative gene expression pattern for a) *E. huxleyi* 217 vs b) *E. huxleyi* 1516 and Rna-seq. list of 9 mM Ca^{2+} relative to 0 mM Ca^{2+}.

Real Time RT-PCR independent validation for *G. oceanica* and *E. huxleyi*

G. oceanica real time RT-PCR was able to independently validate differential expression for 7 of the 10 genes (70%) when compared to the RNA-seq data generated by mapping reads to the transcriptomes (Table 9). The data identified a difference in expression levels for 5/6 genes that were considered upregulated (83%) and 2/4 genes were considered down regulated (50%). *E. huxleyi* strain (217) real time RT-PCR data confirmed only 5 of the 10 genes (50%) of the differentially expressed genes. *E. huxleyi* data found 5/6 genes as being significantly up-regulated (83%). The most significantly differentially expressed gene in both *G. oceanica* and *E. huxleyi* encodes a protein that shows significant homology (e-value =1.38E-147) to a Vomi family protein (46378). When cells were cultured in calcium replicate (9 mM Ca^{2+}) vs. calcium deplete conditions, the Vomi family protein was up-regulated more than 6 and 11- fold in *E. huxleyi* and *G. oceanica*, respectively (Figure 17). The 5 remaining differentially expressed transcripts had an average 2-fold increase for both species (Figures 19, 20).

Real time RT-PCR C_t values were used to verify the statistical significance of difference in expression for a total of 21 genes selected from both RNA-seq. data and to determine the magnitude and direction. Reference normalized C_t values were used as input for a set of pairwise t-tests comparing expression of genes in cells grown in 9 mM and 0 mM calcium conditions. After a Bonferroni correction, real time RT-PCR data showed a total of 17 out of 21 gene (80%) as being statistically differentially expressed. The real time RT-PCR data was in agreement with both RNA-seq. data sets by validating 6 genes as being significantly down regulated and 11 as being significantly up regulated in 9 mM calcium vs. 0 mM calcium (appendix C, D).

Table 9: The relative gene expression pattern between RNA-seq. list blast2go-table_20141106_1156 generated by mapping reads to the transcriptomes and real time RT-PCR analysis using a) *E. huxleyi* (217) and b) *G. oceanica* RNA.

Sequence Name	Protein ID	Hit- Description	*E.H-217*[a]	*G. O*[b]	*RNA- s*
c31156_g1_i13	558392	Type I phosphodiesterase nucleotide pyrophosphatase	UP	UP	UP
c30483_g7_i1	218042	Two component response regulator	Down	Down	UP
c30989_g4_i2	199868	Myosin VI/myosin complex	UP	UP	UP
c13659_g2_i1	365512	Predicted uncharacterized protein LOC104115559	UP	Down	Down
c28658_g1_i4	210744	Clavaminates synthase	UP	Down	Down
c31037_g3_i14	211953	Endoplasmic reticulum mannosyl-oligosaccharide - alpha-mannosidase-like isoform x1	UP	UP	Down
c27445_g3_i9	464892	Hemolysin-related protein	UP	UP	UP
c27886_g1_i2	450163	Beta- aspartyl asparaginyl family	UP	UP	Down
c5364_g1_i1	447372	Endo- -beta-xylanase	UP	UP	UP
c22401_g2_i1	46378	Vomi family protein	UP	UP	UP

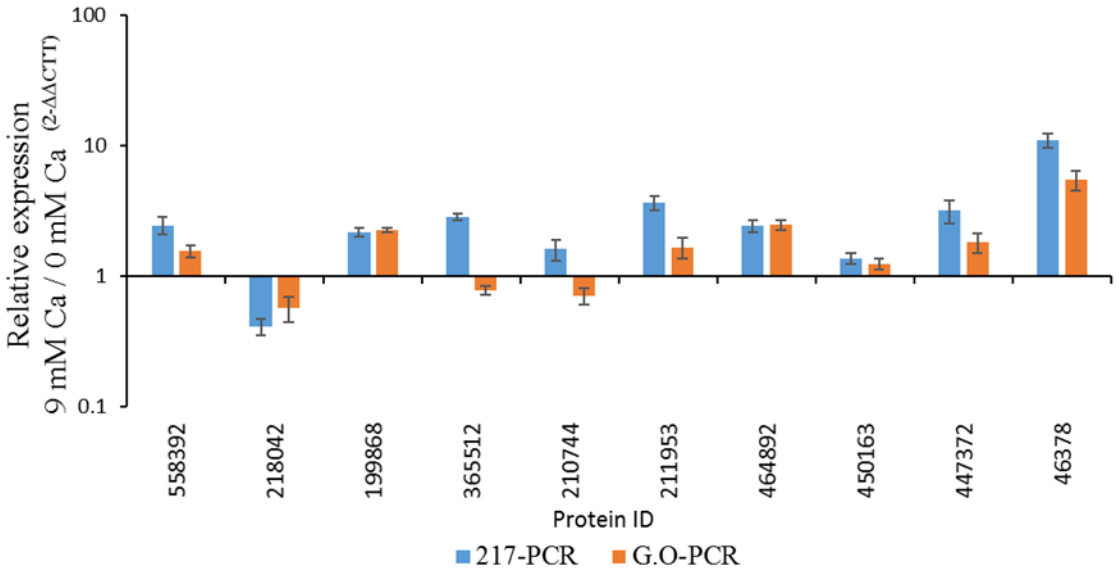

Figure 18: Comparison between *E. huxleyi* (217) and *G.* oceanica real-Time RT-PCR gene expression levels of 9 mM Ca^{2+} relative to 0 mM Ca^{2+}.

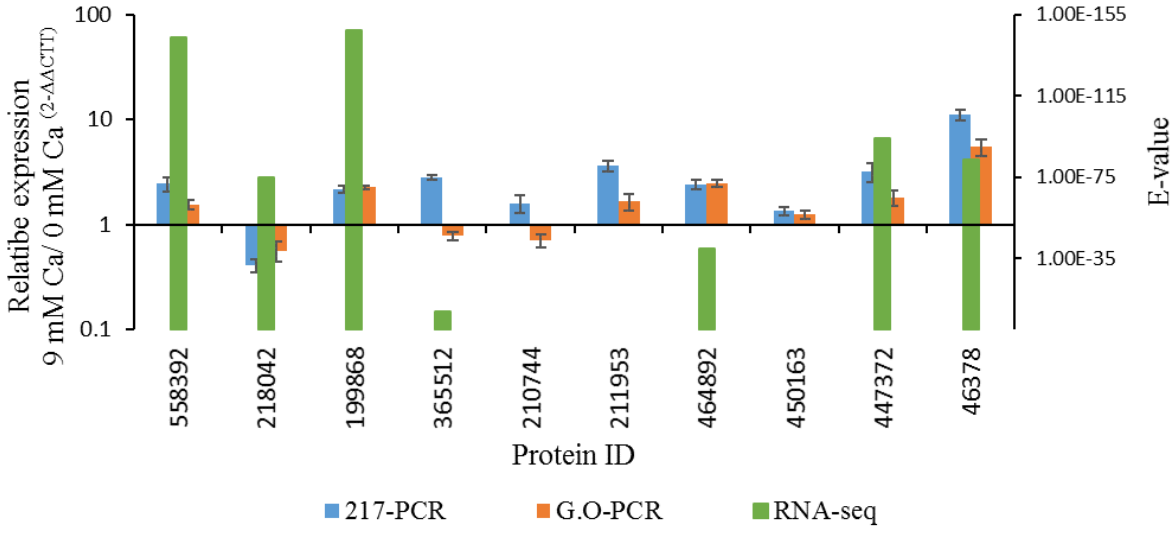

Figure 19: Graphical representation of real-time RT-PCR fold change data for *E. huxleyi* (217) and *G. oceanica* (G. O) (left axis) in comparison to RNA-sequencings list blast2go-table_20141106_1156 E-value generated by mapping reads to the transcriptomes (right axis).

Discussion

Biomineralization plays an important role in the carbon and nutrient cycle of the ocean. Marine phytoplankton are one of the major contributors to the carbon pump (Trimborn et al., 2007). One of the primary forms of biomineralization found in marine plankton is the precipitation of calcium carbonate by coccolithophores. The purpose for coccolith production is still unknown but several hypotheses exist as to their function. These hypotheses include theories that coccoliths protect the alga from predators or viruses, they might be involved in promoting photosynthesis via carbon acquisition (Trimborn et al, 2007), and they allow the organism to move in the water column following nutrients available (Herforta et al., 2004). Even though biomineralization is a very important process in coccolithophorids, the underlying biomineralization mechanism of the process remains unclear.

The aim of this research was to use comparative transcriptomics to identify genes involved in biomineralization. Coccolith forming species *E. huxleyi* and *G. oceanica* and non-coccolith forming species, *I. galbana*, were grown under conditions known to affect biomineralization. Potential calcification genes were selected based on differential expression under conditions that promote or inhibit biomineralization. Therefore, cells were subjected to conditions that enhanced (bicarbonate spike) or inhibited (0 mM Ca^{2+}) coccolith formation. The bicarbonate 'spike' refers to the addition of 20 mM more bicarbonate. Protons in the media react with the bicarbonate and spontaneously equilibrate with CO_2 and H_2O at room temperature: $CO_2 + H_2O \leftrightarrow HCO_3^- + H^+$. The spike helps to trigger biomineralization but is not a substrate for it (Buitenhuis et al., 1999; Herfort et al., 2002). The concentration of the HCO_3^- is unknown and the effects are temporary.

To further understand the biomineralization process within the Isochrysidales clade, this research characterized the physiological parameters of *G. oceanica* including: cell growth, coccolith formation, calcification, and photosynthesis rates in four different growth conditions. The results were then compared to physiological data from *E. huxleyi* and *I. galbana* collected previously by Schroepfer, 2011. The growth data for *G. oceanica* indicated that calcium had a biological impact on cells. Cells that were in calcium rich media (9 mM Ca^{2+}) had a faster doubling time and higher cell density. In addition to playing a role in many physiological processes such as cell signaling, calcium is an essential nutrient in the production of coccoliths. In low concentrations, it reduces calcification and affects coccolith structure which may subsequently affect algal growth (Herfort et al., 2004).

Physiological parameters

Scanning electron microscopy (S.E.M) for *G. oceanica* and *E. huxleyi* revealed that different calcium concentrations significantly impacted coccolith morphology and abundance. Intact, well formed, and normal coccoliths were seen in 9 mM calcium conditions. Under calcium limiting conditions (0 mM Ca^{2+}), however, very few whole coccoliths were visible; coccolith fragments were in discernable amongst the plethora of collapsed cells. In the absence of an intact coccosphere, cells tend to collapse under the vacuum pressures typically use to prepare S.E.M. samples. The results make biological sense as Shiraiwa, 2003, found that calcium concentration influences calcification rate and coccolith morphology by affecting both crystal structure and rate of calcite deposition. Low calcification rates are associated with poor coccolith structure while high calcification rates are associated with well-formed coccoliths. The S.E.M micrographs, however, were not

able to reveal significant coccolith formation differences when samples were treated with 20 mM bicarbonate spike even though sodium bicarbonate has been associated with enhanced calcification and coccolith production (Shiraiwa, 2003).

Calcium titrations and atomic absorption spectroscopy analysis overall showed a significant decrease of calcium in the spent media over time in the 9 mM Ca^{2+} conditions vs. the 0 mM Ca^{2+} condition. Cells from *E. huxleyi* and *G. oceanica* cultures grown under normal calcifying conditions (9 mM Ca^{2+}) were extracting more calcium from the surrounding media over time compared to their non-calcifying counterpart, *I. galbana*. This may suggest that during active calcification, when cells are producing coccoliths, there is higher calcium consumption. Under calcium limiting conditions (0 mM Ca^{2+}) when calcification and coccolithogenesis is expected to be compromised, little if any changes in calcium in the spent media, and no differences across species were observed. All three species had a sudden calcium increase on day 2 for both conditions due to possible calcium introduction during initial culture inoculation process. Cultures for inoculations were grown in normal calcium conditions (9 mM Ca^{2+}).

There was very little difference between calcium titration and atomic absorption spectroscopy for detecting the amount of calcium in the spent media. Calcium titration with EGTA is known to have a precision better than 0.1% (Grasshoff, 1983) while atomic adsorption has a precision of 0.3-1%, the accuracy is 0.5-5%, and the sensitivity is of the order of parts per billion in a gram of a substance (Robinson, 1960; Van Loon, 2012). Determining the titration endpoint readings in the calcium titration method was challenging. As reported by Shin-nan et al., 1997, using a calcium ion selective electrode

as the indicating electrode and a saturated calomel electrode as the reference electrode along with EGTA can reduce observation errors in determining the endpoint and providing better analytical precision less than 0.08%. To directly measure the amount of calcium being used for calcification, the experiment would need to be modified to take two calcium measurements of the same sample: 1) measure the calcium in spent media without the cells and their coccoliths and 2) leaving the cells with their coccoliths in solution and dissolving the coccoliths prior to calcium measurement. The difference in calcium concentration will be the amount of calcium used to form coccoliths. Making these changes may cut down technical variability in future studies.

The link between calcification and photosynthesis has been researched extensively yielding conflicting results. More recent research suggests the two processes are independent (Shiraiwa, 2003; Herfort et al., 2004). Leonardos and colleagues (2009) observed no correlation between photosynthesis and calcification rates or pigment content and coccolith morphology, when *E. huxleyi* cultures were grown under varying light levels in ASW media containing different levels of calcium. Further evidence reveals that photosynthesis is not affected when cells are transferred to calcium free media while calcification is affected by varying calcium concentration (Paasche, 1984; Herfort et al., 2004). As expected, greater estimates of photosynthesis were observed when *G. oceanica* cultures were maintained in ASW with ambient 9 mM versus 0 mM levels of calcium. Calcium replete (9 mM Ca^{2+}) condition had more cells which may have contributed to an overall higher photosynthesis rates over time. When photosynthesis rates are expressed per cell, however, there was a decrease possibly due to increases in cell density which may in turn affect light availability to cells below other cells. Photosynthesis rates per cell were

constant when grown in 0 mM calcium and exhibited significantly slower growth rates and lower cell densities. Photosynthesis rates thus appear to be more closely linked to cell density rather than calcification.

RNA sequencing and Real time RT-PCR

Comparative transcriptomics of haptophytes grown under conditions hypothesized to promote and inhibit biomineralization was used to probe genes and proteins involved in calcification and coccolithogenesis. The list generated by mapping reads to the sequenced genome had an average of 226 hypothetical proteins out of 296 genes while the list mapping the reads to the transcriptome had 18 hypothetical proteins out of 44. Even though more overlap was expected between the lists, there was only one gene in common (hypothetical protein 448086). The small subset of genes that were validated via real time RT-PCR have not been previously identified as genes potentially involved in biomineralization. The list included: Protein 353012 and 240483, which have homology to zinc iron permease proteins and protein 450163 which has a homologous protein in the Beta- aspartyl asparaginyl family. The zinc SLC39 (ZIP) protein family has been found in membranes of secretory vesicles and are responsible for depositing zinc ions into secretory vesicles for exocytosis (Huang et al., 2013) while the beta- aspartyl asparaginyl family contain aspartryl -asparaginyl-B-hydroxylase, which is a hydroxylating enzyme that promotes cell mobility (Silbermann et al., 2010). These genes possibly play a role in biomineralization based on their known cell processes.

RNA-seq data identified a total of 21 genes as being differently expressed, but real time RT-PCR overall only validated a total of 17 genes between *G. oceanica* and *E. huxleyi*, *G. oceanica* RNA independently validated a total of 12 out of 21 genes (57%). Meanwhile

E. huxleyi (217 and 1516) RNA validated a total of 13 out of 21 genes (61%) as being differently expressed when compared to the RNA-seq data. Protein 46378 which shows homology to a vomi family protein was identified as being significantly differentially expressed in both species. Vomi protein families such as Vitelline membrane outer layer protein I have been found in the *Caenorhabditis elegance* genome and are classified as secreted proteins (Suh et al., 2012). Furthermore, vomi protein plays a role in *Drosophila eggshell formation* during stages of vitelline membrane formation (Pascucci et al., 1996). This might suggest that Vomi protein might be involved in the coccolith formation process during calcification. Overall calcification may not have been highly expressed in the selected genes and missed in this analysis. Deep sequencing to increase the number of reads for each sequence genome might help in the future to find higher expression in calcification genes. Also, principal component analysis was used to test the heterogeneity of the transcriptomes and during this process, it become obvious that there was too much variability in the RNA for *I. galbana* samples. Additional RNA extractions for *I. galbana* were sent for additional sequencing and the data is currently still being processed. Once the data is processed, it is expected to help improved data analysis.

New research by Benner and colleagues, 2013, have been able to identify differentially expressed genes that have not been previously investigated but may be involved in calcification. The putative transcripts with homology to fibrilins, which have a Ca^{2+} binding domain, might play a role in signaling pathways that regulate calcification. Other functional groups potentially involved in the calcification processes include: calcium transport, carbonic anhydrases, and inorganic carbon transport. The finding by Benner et al., 2013 helped generate a new RNA-seq. list for *E. huxleyi* 1516 vs 217 grown in 9 mM

calcium and 0 mM calcium (Table 9).The new set of known biomineralization genes in *E. huxleyi* needs to be examined and validated via real time RT-PCR. None of the types of genes described in the above research or in the new set of known biomineralization genes in *E.huxleyi* were found in the current data set analyzed.

In summary, different calcium concentrations (9 mM vs. 0 mM) have a large effect on cells by impacting both growth and calcification. Coccolith formation is found to be impacted by calcium conditions, consistent with previous studies (Leonardos et al., 2009). Calcium titration and atomic absorption spectroscopy analyses were found to be similar when used as indirect estimates of calcification. Calcium conditions were found to have an impact on biomineralization expression. It was also found that calcification and photosynthesis are independent processes and are not coupled, consistent with Herfort et al., (2004). Even though RNA sequencing technology with real time RT-PCR validation should be accurate and reproducible molecular techniques for determining genes expression, this research was only able to validate 57 % of the genes using *G. oceanica* and 61% of the genes using *E. huxleyi* from the RNA-seq. data. Future research can use this study as an outline to identifying genes potentially involved in biomineralization in *E. huxleyi* and *G. oceanica*.

Future Direction

While this study highlights new information about biomineralization in coccolithophores and studied a number of genes and proteins which are potentially involved in this complex process, further studies are necessary to confirm and elucidate the role of these genes and proteins. The data in this study analyzed 10 differentially expressed genes from the 44 genes in the current RNA-seq. list generated via mapping to the

transcriptome. There remain an additional 34 genes that require additional validation via real time RT-PCR. To further elucidate the genes involved in biomineralization, the transcriptomes should be used to analyze the response the cells had to the sodium bicarbonate spiked conditions. Changes in gene expression across treatments will reflect the pleiotropic effects of sodium bicarbonate on the cells which can further narrow down the genes involved in biomineralization.

In this context of the current research focusing and narrowing down potential genes involved in biomineralization, it is clear that a transformation system for *E. huxleyi* is urgently need to validate, determine the subcellular localization, and functionally characterize the role of the proteins encoded by these candidate biomineralization genes. The availability of a transformation system for *E. huxleyi* will facilitate functional genomics efforts enabling genes to be "knocked out", over expressed and tagged with fluorescent proteins. More recently, similarities between *E. huxleyi* calcifying (217) and non-calcifying (1516) strains have been highlighted. In light of this information, having a transformation system for *E. huxleyi* will provides an opportunity for examining the epigenome of strains CCMP 1516 and PLY 217. At this point it is unclear whether a single nucleotide mutation or DNA methylation affected 1516 ability to calcify by silencing or turning it off genes. With a transformation system, further studies will be able to identify which genes are vital to the biomineralization process in coccolithophores.

Table 10: List of known biomineralization genes in *E. huxleyi* 1516 grown in 9mM and 0 mM calcium conditions and their expression value based on RNA-seq. data.

ID	Gene Description	E.hux-1516_0 Ca^{2+}	E.hux-1516_9 Ca^{2+}	E. hux 217_0 Ca Ca^{2+}	E.hux-217_9 Ca^{2+}
416800	Ca2+/H+ exchanger (CAX3) (CAX family)	32.02	5.07	15.22	5
448526	four domain voltage-gated Ca2+ channels	1.57	0.3	1.28	0.81
72273	cation/H+ exchanger (CAX family)	0.6	0.18	1.2	0.37
203920	cation/Ca2+exchanger	1.18	0.18	0.96	0.52
107737	Ca2+/Mg2+-permeable cation channels transient receptor potential	152.14	162.39	35.46	61.01
460292	Ca2+/Mg2+-permeable cation channels (LTRPC family)	261.2	256.92	55.85	92.66
463266	fibrillins and related proteins containing Ca2+-binding EGF-like domains	17.37	13.25	62.33	69.14
431830	GPA (glutamic acid, proline and alanine) unknown, calcium binding	588.27	908.88	191.73	270.58
437452	carbonic anhydrase, alpha	45.6	128.66	37.14	85.84
456048	carbonic anhydrase, alpha	0.93	0.17	0.91	1.62
469783	carbonic anhydrase, delta	2.03	0.45	1.71	1.11
436031	carbonic anhydrase, delta	106.32	19.55	58.33	33.3
373149	carbonic anhydrase, gamma	10.07	3.78	14.97	7.74
432493	carbonic anhydrase, gamma	14.18	4.36	17.84	6.29
200137	bicarbonate transporter	14.5	5.12	19.65	9.34
469783	bicarbonate transporter	2.03	0.45	1.71	1.11
198643	anion exchanger-like (AEL1), SLC4 family of solute carrier proteins	0.78	0	3.16	1.4
99943	anion exchanger-like, SLC4 Na+ independent Cl-/HCO3- exchangers	3.67	1.08	8.49	3.28
359783	subunit of Vo sector of a vacuolar H+-ATPase	83.97	14.67	50.23	14.26
67081	plasma membrane type H pump/ATPase (PM H+ ATPase)	0.69	0.28	0.23	0.11
439538	V-ATPase, A	25.52	3.82	21.52	6.05
435128	V-ATPase, B	38.49	4.55	56.02	16.07
413949	V-ATPase, D	24.13	9.54	45.24	35.65
433060	V-ATPase, E	60.69	12.51	66.01	20.86

References

1. **Ansorge, W. J.** 2009. Next-generation DNA sequencing techniques. New Biotechnology **25:**195-203.

2. **Arya, M., I. S. Shergill, M. Williamson, L. Gommersall, N. Arya, and H. R. Patel.** 2005. Basic principles of real-time quantitative PCR. Expert review of molecular diagnostics **5:**209-219.

3. **Benner, I., R. E. Diner, S. C. Lefebvre, D. Li, T. Komada, E. J. Carpenter, and J. H. Stillman.** 2013. Emiliania huxleyi increases calcification but not expression of calcification-related genes in long-term exposure to elevated temperature and pCO2. Philosophical Transactions of the Royal Society B: Biological Sciences **368:**20130049.

4. **Bollmann, J.** 1997. Morphology and biogeography of *Gephyrocapsa* coccoliths in Holoene sediments. Marine Micropaleontology **29:**319-350.

5. **Bollmann, J., K. H. Baumann, and H. R. Thierstein.** 1998. Global dominance of *Gephyrocapsa* coccoliths in the Late Pleistocene: Selective dissolution, evolution, or global environmental change? Paleoceanography **13:**517-529.

6. **Brown, C. W., and J. A. Yoder.** 1994. Coccolithophorid blooms in the global ocean. Journal of Geophysical Research **99:**7467-7467.

7. **Buitenhuis, E. T., H. J. De Baar, and M. J. Veldhuis.** 1999. Photosynthesis and calcification by Emiliania huxleyi (Prymnesiophyceae) as a function of inorganic carbon species. Journal of Phycology **35:**949-959.

8. **Chisholm, J. R. M., and J.-P. Gattuso.** 1991. Validation of the Alkalinity Anomaly Technique for Investigating Calcification and Photosynthesis in Coral Reef Communities. Limnology and Oceanography **36:**1232-1239.

9. **Corstjens, P. L., A. Van Der Kooij, C. Linschooten, G. J. Brouwers, P. Westbroek, and E. W. Jong.** 1998. GPA, a calcium-binding protein in the coccolithophorid *Emilliania huxleyi* (Prymnesiophyceae). Journal of Phycology **34:**622-630.

10. **Edvardsen, B., W. Eikrem, J. Green, R. A. Andersen, S. Y. Moon-van der Staay, and L. K. Medlin.** 2000. Phylogenetic reconstructions of the Haptophyta inferred from 18S ribosomal DNA sequences and available morphological data. Phycologia **39:**19-35.

11. **Fujiwara, S., M. Sawada, J. Someya, N. Minaka, M. Kawachi, and I. Inouye.** 1994. Molecular phylogenetic analysis of rbcL in the Prymnesiophyta. Journal of Phycology **30:**863-871.

Reference continuation

12. **Giachelli, C.** 2005. Inducers and inhibitors of biomineralization: lessons from pathological calcification. Orthodontics & craniofacial research **8:**229-231.

13. **Gopinathan, C.** 1984. Growth characteristics of some nannoplankters. Journal of the Marine Biological Association of India **26:**89-94.

14. **Gordon, R., and J. Parkinson.** 2005. Potential Roles for Diatomists in Nanotechnology. Journal of Nanoscience and Nanotechnology **5:**35-40.

15. **Green, J. C., Course,P.A, and Tarran,G.A.** 1996. The life-cycle of *Emiliania huxleyi*: A brief review and a study of relative ploidy levels analysed by flow cytometry. Journal of Marine Systems **9:**44.

16. **Guillard, R. R. L.** 1975. Culture of phytoplankton for feeding marine invertebrates. *In Culture of Marine Invertebrate Animals*. Smith W, L and Chanley M, H (Eds.). pp 26-60. Plenum Press, New York.

17. **Henriksen, K., and S. L. S. Stipp.** 2009. Controlling biomineralization: The effect of solution composition on coccolith polysaccharide functionality. Crystal Growth and Design **9:**2088-2097.

18. **Herfort, L., E. Loste, F. Meldrum, and B. Thake.** 2004. Structural and physiological effects of calcium and magnesium in *Emiliania huxleyi* (Lohmann) Hay and Mohler. Journal of structural biology **148:**307-314.

19. **Herfort, L., Thake,B, and Roberts, J.** 2002. Acquisition and use of bicarbonate by Emiliania huxleyi. New Phytologist **156:**427-436.

20. **Holligan, P. M., E. Fernández, J. Aiken, W. M. Balch, P. Boyd, P. H. Burkill, M. Finch, S. B. Groom, G. Malin, and K. Muller.** 1993. A biogeochemical study of the coccolithophore, *Emiliania huxleyi*, in the North Atlantic. Global Biogeochemical Cycles **7:**879-900.

21. **Hornshøj, H., E. Bendixen, L. N. Conley, P. K. Andersen, J. Hedegaard, F. Panitz, and C. Bendixen.** 2009. Transcriptomic and proteomic profiling of two porcine tissues using high-throughput technologies. BMC genomics **10:**30.

22. **Huang, L., and S. Tepaamorndech.** 2013. The SLC30 family of zinc transporters – A review of current understanding of their biological and pathophysiological roles. Molecular Aspects of Medicine **34:**548-560.

23. **Inouye, I.** 1997. Systematics of Haptophyte Algae in Asia-Pacific Waters. Algae (The Korean Journal of Phycology) **12:**247-261.

24. **Keller, M., Selvin, R.C, Claus, W., and Guillard, R. R.** 1987. Media for the culture of oceanic ultraphytoplankton. Journal of Phycology **23:**633-638.

25. **Klaveness, D.** 1972. Coccolithus huxleyi (Lohm.) Kamptn II. The flagellate cell, aberrant cell types, vegetative propagation and life cycles. British Phycological Journal **7:**309-318.

26. **Kremling, K.** 1983. Determination of the major constituents. *In Methods of Sea water Analysis*. Grasshoff, K, Ehrhardt, M and Kremling, (Eds.). pp 247-252. Verlag Chemie, Weinheim.

27. **Langer, G., L. J. de Nooijer, and K. Oetjen.** 2010. On the role of the cytoskeleton in coccolith morphogenesis: the effect of cytoskeleton inhibitors. Journal of Phycology **46:**1252-1256.

28. **Leonardos, N., B. Read, B. Thake, and J. R. Young.** 2009. No Mechanistic Dependence of Photosynthesis on Calcification in the Coccolithophorid *Emiliania Huxleyi*(Haptophyta). Journal of Phycology **45:**1046-1051.

29. **Lister, R., R. C. O'Malley, J. Tonti-Filippini, B. D. Gregory, C. C. Berry, A. H. Millar, and J. R. Ecker.** 2008. Highly integrated single-base resolution maps of the epigenome in Arabidopsis. Cell **133:**523-536.

30. **Livak, K. J., and T. D. Schmittgen.** 2001. Analysis of Relative Gene Expression Data Using Real-Time Quantitative PCR and the $2^{-\Delta\Delta CT}$ Method. Methods **25:**402-408.

31. **Livingston, B. T., C. E. Killian, F. Wilt, A. Cameron, M. J. Landrum, O. Ermolaeva, V. Sapojnikov, D. R. Maglott, A. M. Buchanan, and C. A. Ettensohn.** 2006. A genome-wide analysis of biomineralization-related proteins in the sea urchin *Strongylocentrotus purpuratus*. Developmental Biology **300:**335-348.

32. **Mann, S.** 2001. Biomineralization principles and concepts in bioinorganic materials chemistry, vol. 5. Oxford University Press Inc., New York, pp 6-8.

33. **Moheimani, N. R., and M. A. Borowitzka.** 2011. Increased CO2 and the effect of pH on growth and calcification of *Pleurochrysis carterae* and *Emiliania huxleyi* (Haptophyta) in semicontinuous cultures. Applied microbiology and biotechnology **90:**1399-1407.

34. **Moolna, A., and R. E. Rickaby.** 2012. Interaction of the coccolithophore Gephyrocapsa oceanica with its carbon environment: response to a recreated high-CO(2) geological past. Geobiology **10:**72-81.

Reference continuation

35. **Mutz, K.-O., A. Heilkenbrinker, M. Lönne, J.-G. Walter, and F. Stahl.** 2013. Transcriptome analysis using next-generation sequencing. Current opinion in biotechnology **24:**22-30.

36. **Nagalakshmi, U., Z. Wang, K. Waern, C. Shou, D. Raha, M. Gerstein, and M. Snyder.** 2008. The transcriptional landscape of the yeast genome defined by RNA sequencing. Science **320:**1344-1349.

37. **Nagasawa, H.** 2004. Macromolecules in biominerals of aquatic organisms. Thalassas: An international journal of marine sciences **20:**15-24.

38. **Nguyen, B., R. M. Bowers, T. M. Wahlund, and B. A. Read.** 2005. Suppressive subtractive hybridization of and differences in gene expression content of calcifying and noncalcifying cultures of *Emiliania huxleyi* strain 1516. Applied and environmental microbiology **71:**2564-2575.

39. **Okazaki, M., S. Sakuda, N. Ozaki, T. Kogure, and H. Nagasawa.** 2004. Structural and Functional Diversity of Acidic Polysaccharides from Various Species of Coocolithophorid Algae. Thalassas: An international journal of marine sciences **20:**59-68.

40. **Paasche, E.** 2001. A review of the coccolithophorid Emiliania huxleyi (Prymnesiophyceae), with particular reference to growth, coccolith formation, and calcification-photosynthesis interactions. Phycologia **40:**503-529.

41. **Paasche, E.** 1998. Roles of nitrogen and phosphorus in coccolith formation in Emiliania huxleyi (Prymnesiophyceae). European Journal of Phycology **33:**33-42.

42. **Park, S. C.** 2013. Towards an understanding of biomineralization using comparative transcriptomics in three sisters species of coccolithophorids. Master's thesis. California State University, San Marcos **1:**1-70.

43. **Pascucci, T., J. Perrino, A. Mahowald, and G. Waring.** 1996. Eggshell Assembly inDrosophila: Processing and Localization of Vitelline Membrane and Chorion Proteins. Developmental Biology **177:**590-598.

44. **Rhodes, L. L., B. M. Peake, A. L. MacKenzie, and S. Marwick.** 1995. Coccolithophores *Gephyrocapsa oceanica* and *Emiliania huxleyi* (Prymnesiophyceae = Haptophyceae) in New Zealand's coastal waters: Characteristics of blooms and growth in laboratory culture. New Zealand Journal of Marine and Freshwater Research **29:**345-357.

45. **Robinson, J.** 1960. Atomic absorption spectroscopy. Analytical chemistry **32:**17A-29A.

46. **Schroepfer, C.** 2011. Identification of potential biomineralization linked genes in Emiliania huxleyi via high-throughput sequencing with RT-PCR verification, as well as annotation of cyclophilin gene models. Master's Thesis. California State University, San Marcos.

47. **Shiraiwa, Y.** 2003. Physiological regulation of carbon fixation in the photosynthesis and calcification of coccolithophorids. Comparative Biochemistry and Physiology Part B: Biochemistry and Molecular Biology **136:**775-783.

48. **Sikes, C. S., R. D. Roer, and K. M. Wilbur.** 1980. Photosynthesis and coccolith formation: Inorganic carbon sources and net inorganic reaction of deposition1. Limnology and Oceanography **25:**248-261.

49. **Sikes, S. C., and K. M. Wilbur.** 1982. Functions of coccolith formation. American Society of Limnology and Oceanography **27:**18-26.

50. **Silbermann, E., P. Moskal, N. Bowling, M. Tong, and S. M. de la Monte.** 2010. Role of aspartyl-(asparaginyl)-β-hydroxylase mediated notch signaling in cerebellar development and function. Behavioral and Brain Functions **6:**68.

51. **Sorrosa, J. M., M. Satoh, and Y. Shiraiwa.** 2005. Low temperature stimulates cell enlargement and intracellular calcification of coccolithophorids. Mar Biotechnol (NY) **7:**128-133.

52. **Soto, A. R., H. Zheng, D. Shoemaker, J. Rodriguez, B. A. Read, and T. M. Wahlund.** 2006. Identification and preliminary characterization of two cDNAs encoding unique carbonic anhydrases from the marine alga *Emiliania huxleyi*. Applied and environmental microbiology **72:**5500-5511.

53. **Stanley, S. M.** 2008. Effects of global seawater chemistry on biomineralization: past, present, and future. Chemical reviews **108:**4483-4498.

54. **Strommer, J., R. Gregerson, M. Vayda, B. Glick, and J. Thompson.** 1993. Isolation and characterization of plant mRNA. *In Methods in Plant Molecular Biology and Biotechnology*. Glick, B, R and Thompson, J, E (Eds.). pp 49-66.CRC Press, Boca Raton.

55. **Suffrian, K., K. G. Schulz, M. A. Gutowska, U. Riebesell, and M. Bleich.** 2011. Cellular pH measurements in *Emiliania huxleyi* reveal pronounced membrane proton permeability. The New phytologist **190:**595-608.

56. **Suh, J., and H. Hutter.** 2012. A survey of putative secreted and transmembrane proteins encoded in the C. elegans genome. BMC genomics **13:**333.

Reference continuation

57. **Trimborn, S., Longer,G and Rost, B.** 2007. Effects of varing calcium concentrations and light intensity on calcification and photosynthesis in *Emiliania huxleyi*. American Society of Limnology and Oceanography **52:**2285-2293.

58. **Van Loon, J. A.** 2012. Analytical atomic absorption spectroscopy: selected methods. Elsevier.

59. **Vera, J. C., C. W. Wheat, H. W. Fescemyer, M. J. Frilander, D. L. Crawford, I. Hanski, and J. H. Marden.** 2008. Rapid transcriptome characterization for a nonmodel organism using 454 pyrosequencing. Molecular ecology **17:**1636-1647.

60. **Weiner, S., and P. M. Dove.** 2003. An overview of biomineralization processes and the problem of the vital effect. Reviews in Mineralogy and Geochemistry **54:**1-29.

61. **Westbroek, P., Christopher W., Bleijswijk, J. V, Brownlee, C., Brummer, G.J. et al.** 1993. A model system approach to biological climate forcing. The example of *Emiliania huxleyi*. Global and planetary change **8:**27-46.

62. **Westbroek, P., E. De Jong, P. Van der Wal, A. Borman, J. De Vrind, D. Kok, W. De Bruijn, and S. Parker.** 1984. Mechanism of calcification in the marine alga *Emiliania huxleyi* [and Discussion]. Philosophical Transactions of the Royal Society B: Biological Sciences **304:**435-444.

63. **Yamamoto, M., Y. Shiraiwa, and I. Inouye.** 2000. Physiological responses of lipids in Emiliania huxleyi and Gephyrocapsa oceanica (Haptophyceae) to growth status and their implications for alkenone paleothermometry. Organic Geochemistry **31:**799-811.

64. **Young, J. R.** 1994. Functions of coccoliths. *In Coccolithophores.* Winter, A, and William, G,S (Eds.). pp 17-21, 29-32,39-40,46,63-69,179-180. Cambridge University Press, New York.

65. **Young, J. R., S. A. Davis, P. R. Bown, and S. Mann.** 1999. Coccolith ultrastructure and biomineralisation. Journal of structural biology **126:**195-215.

66. **Young, J. R., J. M. Didymus, P. R. Brown, B. Prins, and S. Mann.** 1992. Crystal assembly and phylogenetic evolution in heterococcoliths. Nature **356:**516-518.

67. **Young, J. R., and K. Henriksen.** 2003. Biomineralization within vesicles: The calcite of coccoliths. Reviews in mineralogy and geochemistry **54:**189-215

APPENDICES

APPENDIX A. Transcriptome assembly for all three species through Trinity.

	E. huxleyi	*G. oceanica*	*I. galbana*
Size (mega bases)	47.47	62.84	38.52
Number of transcripts	67797	77634	47517
Number of genes	43694	43375	38083
Min length of sequences	201	201	201
Average	700	809	811
N50	954	1093	1139
Max	10764	9149	14713

APPENDIX B. Primer sets for Real-Time PCR.

Protein ID	Forward (5' to 3')	Reverse (5' to 3')	Product GC%	Product Length	Expected Tm	Actual Tm
230169	ACATCTTCGACCTCGTCACC	TCGTATATGCCGAGCGAGTT	58	181	86.23	85.40
215610	TGCAGTTCTCCACAAAGGTG	GCGACATGAAGGTCTCGTTC	67	162	87.66	86.07
107263	GAGGACGACAACGAGGTGAC	CATGGTTGACGCCAGAGAC	61	120	80.65	79.07
100838	CGTCGCCAAGAAGAATGG	GATCCGCCTCTTGACCTTG	67	109	87.20	86.32
199016	ATGGACCTGCTGCACGAT	GATCCGCCTCTTGACCTTG	63	138	87.51	88.07
353012	GACTTGGTGCTCGGCTACTT	GACCAGCGAGTAGGAGGACA	64	129	86.87	85.50
103255	GTGCAGGACAAGAGCAACAA	GCGTCATGTCAGTGAGAAGG	50	139	85.56	84.37
240483	TGGCAGGAGAATGTGGTGTA	ACTGAGGTGAGCTTGGTCGT	65	245	84.78	83.33
46343	TGCAGATGTACTGCGGATCT	CATTCATTGCGGTATCGTC	63	154	87.98	88.17
432991	CAGAACCAGCCTCGTCGTA	GTGAGGATCGTGGTCGAGAT	63	192	86.28	85.78
222767	AGATCCAGATTGCGTACAAGC	ATGCGGAACTTGACATTGTG	62	130	86.47	86.78
558392	AGTTCGCTCTGGCAGTCAA	AAGCTGTAGAAGCGGTCGAG	69	223	87.49	87.25
218042	GTTGTGGAGGACGACGAGAT	GGAGATCGTAGCCGTTCAAG	66	208	86.89	84.96
199868	GACGGACCAGAACAACAACC	CGTCCAGCTCATCTCTCTCC	68	145	88.61	87.96
365512	GACGGCTCGATCAACAAGA	CCGTTCGGAGAGCTTCAGT	66	101	87.20	87.83
210744	GAGGACTGTGTTGTGCCTGA	GAGGACTGTGTTGTGCCTGA	63	210	88.52	87.96
211953	CTGCAACAACAGCAGGTACG	CACTTGCCACTTGTCCACAC	58	129	87.85	86.25
464892	CCGAGAACATCAACAAGCAG	GAAGAAGTCCATGCGAGAGG	60	158	84.53	83.71
450163	AAGACGTTGCCGCTCTGT	GAGCCATCGACGAGAAGAAG	65	127	87.08	86.75
447372	AGTACGACGGCACCTTCATC	AGCTTCTTGGCCTCCTCCT	66	100	87.35	86.17
46378	TGCAGATGTACTGCGGATCT	TCATTCATTGCGGTATCGTC	62	154	87.54	86.42
HK447254	GGAGTACGACTCGGAGATGC	TACTCGGGCAAGTCCTCATC	64	229	88.0	87.80

Appendix C: Two tail t-test results for real time RT-PCR comparing 9 mM vs. 0 mM calcium conditions. Statistical significance of differential expression based on p-value (0.004) after Bonferroni correction. Magnitude and direction for Real time RT-PCR fold change (F.D). RNA-seq. Geph_DE0V9_padj0.1_in-ehux-not-iso gene list data generated by mapping reads to the genome.

Protein ID	*P-value 217*	F.D -217	*P-value G. o*	*F.D- G. o*	*P-value 1516*	F.D -1516	Hit- Description
103255	0.053	8.7 +	0.003	0.1 -	0.028	4.2 +	Chaperone protein
199016	0.013	5.5 +	0.002	0.4 -	0.006	2.5 +	Translation initiation Factor IF-2
353012	0.022	3.1 +	0.545	4.4 +	0.004	0.3 -	Zinc iron permease
240483	0.018	6.0 +	0.342	4.4 +	0.001	0.3 -	Zinc iron permease
222767	0.012	8.6 +	0.876	3.6 +	0.016	2.6 +	Rtx toxin/ATPase binding
46343	0.002	17.5 +	0.002	4.7 +	0.002	3.4 +	Membrane protein
432991	0.001	9.5 +	0.013	0.3 -	0.299	0.4 -	Membrane protein
230169	0.001	6.4 +	0.019	0.4 -	0.301	0.6 -	Protein Kinase domain
100838	0.003	7.7 +	0.001	4.0 +	0.035	0.4 -	Hypothetical protein
215610	0.001	4.3 +	0.003	3.8 +	0.743	0.6 -	Hypothetical protein
107263	0.002	3.1 +	0.022	0.2 -	0.003	1.8 +	Hypothetical protein

Appendix D: RNA-seq. list blast2go-table_20141106_1156 list generated by mapping reads to the transcriptomes: Two tail t-test results for real time RT-PCR comparing 9 mM vs. 0 mM calcium conditions. Statistical significance of differential expression based on p-value (0.004) after Bonferroni correction. Magnitude and direction for Real time RT-PCR fold change (F.D).

Protein ID	*P-value 217*	F.D -217	*P-value G. o*	*F.D- G. o*	Hit- Description
558392	0.004	1.6 +	0.002	2.44 +	Type I phosphodiesterase nucleotide pyrophosphatase
218042	0.870	0.6 -	0.051	0.41 -	Two component response regulator
199868	0.003	2.3 +	0.001	2.16 +	Myosin VI/myosin complex
365512	0.021	0.8 +	0.002	2.83 -	Predicted uncharacterized protein LOC104115559
210744	0.007	0.7 +	0.001	1.60 -	Clavaminates synthase
211953	0.318	1.7 +	0.078	3.63 +	Endoplasmic reticulum mannosyl-oligosaccharide -alpha-mannosidase-like isoform x1
464892	0.003	2.5 +	0.004	2.41 +	Hemolysin-related protein
450163	0.093	1.2 +	0.637	1.35 +	Beta- aspartyl asparaginyl family
447372	0.003	1.8 +	0.003	3.17 +	Endo- -beta-xylanase
46378	0.004	5.5 +	0.002	11.00 +	Vomi family protein

APPENDIX E: RNA-seq. blast2go-table_20141106_1156 gene list generated by mapping reads to the transcriptomes.

Seq. Name		Seq. Description	Seq. Length	#Hits	min. eValue
c31156_g1_i13	jgi|Emihu1|197656|	pyrophosphatase	2555	20	1.39E-144
c30483_g7_i1	jgi|Emihu1|218042|	two component response regulator	2251	20	9.63E-76
c30989_g4_i2	jgi|Emihu1|100780|	myosin vi	5562	20	1.38E-147
c13659_g2_i1		LOC104115559	1271	7	1.76E-09
c28658_g1_i4	jgi|Emihu1|416307|	clavaminate synthase	1603	20	0
c31037_g3_i14	jgi|Emihu1|211954|	oligosaccharide -alpha-mannosidase-like	5268	20	0
c23352_g1_i2		hypothetical protein PRUPE_ppa018860mg	2272	20	2.31E-40
c27445_g3_i9	jgi|Emihu1|464911|	hemolysin-related protein	3231	20	0
c27886_g1_i2	jgi|Emihu1|450163|	beta-aspartyl asparaginyl family	1336	20	0
c5364_g1_i1	jgi|Emihu1|431720|	endo--beta-xylanase	1643	20	4.56E-95
c22401_g2_i1	jgi|Emihu1|46378|g	vomi family protein	2593	20	1.86E-84
c26186_g1_i3	jgi|Emihu1|108724|	phosphoglycerate mutase family protein	3597	20	1.50E-121
c27862_g1_i5	jgi|Emihu1|440641|	glycosyltransferase family 77 protein	3258	20	8.79E-100
c28090_g2_i3	jgi|Emihu1|446781|	protein	4372	20	2.20E-154
c29829_g6_i8	jgi|Emihu1|454811|	dna ligase	3923	20	0
c30302_g8_i10	jgi|Emihu1|443563|	homolog 3	2102	20	5.45E-42
c31156_g1_i12	jgi|Emihu1|197656|	phosphodiesterase	2818	20	1.37E-143
c10254_g1_i2	jgi|Emihu1|439276|	hypothetical protein EMIHUDRAFT_360439	1685	2	3.37E-62
c11315_g1_i1		---NA---	696	0	
c14149_g1_i3		---NA---	3582	0	
c16275_g1_i1		---NA---	1356	0	
c18320_g1_i1	jgi|Emihu1|440222|	hypothetical protein EMIHUDRAFT_440222	1760	3	0
c18521_g1_i1		2013359a transposase	1377	14	7.22E-07
c23207_g1_i2	jgi|Emihu1|470551|	hypothetical protein EMIHUDRAFT_470551	2530	3	3.87E-173
c23219_g1_i11	jgi|Emihu1|432080|	hypothetical protein EMIHUDRAFT_432080	2415	1	1.78E-93
c23219_g1_i14	jgi|Emihu1|432080|	hypothetical protein EMIHUDRAFT_432080	2301	1	1.86E-93
c27186_g2_i1		protein	1167	4	4.74E-15
c28636_g6_i2	jgi|Emihu1|432843	hypothetical protein EMIHUDRAFT_432843	1695	2	3.11E-130
c28648_g1_i9	jgi|Emihu1|455112|	hypothetical protein EMIHUDRAFT_455112	1681	20	1.14E-129
c29213_g1_i1		---NA---	804	0	
c29310_g1_i4	jgi|Emihu1|361805|	hypothetical protein EMIHUDRAFT_110455	2590	6	4.98E-138
c29455_g1_i11	jgi|Emihu1|436896|	hypothetical protein EMIHUDRAFT_252958	2566	6	6.32E-139
c29487_g1_i4	jgi|Emihu1|360367|	hypothetical protein EMIHUDRAFT_360367	1821	2	3.19E-74
c29941_g5_i2	jgi|Emihu1|448086|	partial	1469	2	2.57E-62
c30267_g2_i14	jgi|Emihu1|351425|	hypothetical protein EMIHUDRAFT_351425	1237	1	8.31E-123
c30390_g1_i5	jgi|Emihu1|459937|	hypothetical protein EMIHUDRAFT_459937	1972	2	1.26E-102
c30688_g5_i1	jgi|Emihu1|459192|	hypothetical protein EMIHUDRAFT_448970	1412	3	0
c30688_g5_i5	jgi|Emihu1|459192|	hypothetical protein EMIHUDRAFT_448970	1475	3	0
c30914_g1_i11	jgi|Emihu1|462848|	---NA---	3111	0	
c30933_g7_i2	jgi|Emihu1|432978|	membrane protein	767	11	7.37E-147
c30973_g1_i1		---NA---	1057	0	
c33631_g1_i1		protein	1377	8	1.69E-29
c40046_g1_i1		hypothetical protein EMIHUDRAFT_210724	1044	2	8.66E-69
c7977_g1_i2		hypothetical protein EMIHUDRAFT_421474	859	1	4.13E-17

APPENDIX F: RNA-seq. Geph_DE0V9_padj0.1_in-ehux-not-iso gene list data generated by mapping reads to the genome.

ID	baseMean	log2FoldChange	lfcSE	stat	pvalue	padj	evalue
evm.model.Contig0.42	3623.21262	1.408894706	0.468163734	3.009405907	0.00261759	0.06199186	0
evm.model.Contig1.51	142.837553	-2.07752505	0.67589459	-3.073741209	0.00211393	0.05264541	7.18E-134
evm.model.Contig1.52	90.7696108	-1.8233879	0.609437778	-2.991918071	0.00277231	0.06477031	1.01E-90
evm.model.Contig10.10	675.455736	1.610765067	0.521166904	3.090689479	0.00199692	0.05033507	2.89E-161
evm.model.Contig1001.49	168.055201	-1.89766162	0.600611163	-3.159551025	0.00158012	0.04318313	5.98E-37
evm.model.Contig1002.13	22.796947	-2.13350406	0.704689421	-3.02758066	0.0024652	0.05933046	3.99E-38
evm.model.Contig1005.11	14.1081209	-2.62024022	0.762370985	-3.436962153	0.00058828	0.02077981	3.48E-20
evm.model.Contig1014.2	308.903854	-2.22724553	0.556968705	-3.998870144	6.36E-05	0.00379862	4.09E-32
evm.model.Contig1019.29	61.3629748	-3.17904097	0.610107254	-5.210626402	1.88E-07	3.64E-05	2.01E-32
evm.model.Contig1020.21	256.717038	-2.23288642	0.523887901	-4.262145432	2.02E-05	0.00152369	6.73E-67
evm.model.Contig1030.8	1141.71856	-1.72768493	0.503036748	-3.434510371	0.00059363	0.0209331	1.64E-56
evm.model.Contig1031.22	30882.0764	1.420818358	0.508473903	2.794279806	0.00520155	0.09732981	5.01E-93
evm.model.Contig1031.34	1895.13788	1.368659864	0.461173832	2.96777434	0.00299964	0.06802824	1.45E-40
evm.model.Contig1035.13	30.4401459	-2.05246731	0.655061251	-3.133244873	0.00172885	0.04603621	2.06E-104
evm.model.Contig1037.26	4767.99681	-2.55923229	0.430612968	-5.943230873	2.79E-09	1.76E-06	0
evm.model.Contig1037.27	97.697904	-2.11728248	0.529323214	-3.999980395	6.33E-05	0.00379174	2.67E-11
evm.model.Contig1039.21	84.926742	2.618289355	0.549653779	4.7635247	1.90E-06	0.00023803	8.31E-46
evm.model.Contig1041.5	38.5687613	-2.85354102	0.650321192	-4.387894873	1.14E-05	0.00097827	4.21E-131
evm.model.Contig105.13	215.765671	2.425402508	0.554202392	4.376384046	1.21E-05	0.00102431	2.64E-29
evm.model.Contig1052.9	139.762866	-1.5269777	0.511255138	-2.986723431	0.00281985	0.06522074	1.05E-22
evm.model.Contig1056.37	43.9600007	-2.50970073	0.686781981	-3.654290303	0.00025789	0.01120599	2.59E-97
evm.model.Contig1059.6	165.684314	-1.87521557	0.496742722	-3.77502375	0.00015999	0.00791201	2.69E-86
evm.model.Contig1073.19	1310.61532	1.291249122	0.462702402	2.790668726	0.00525993	0.0978931	0
evm.model.Contig1073.27	114.795386	-2.55375255	0.623594143	-4.095215746	4.22E-05	0.00278196	-
evm.model.Contig1082.47	340.113329	1.941917634	0.576264687	3.369836251	0.00075213	0.02515574	1.57E-103
evm.model.Contig11.19	306.104826	2.188079005	0.515929848	4.241039773	2.22E-05	0.0016445	2.71E-148
evm.model.Contig11.47	214.06752	1.624945281	0.581342093	2.795161923	0.00518737	0.09732981	6.19E-85
evm.model.Contig1103.10	61.514579	-3.18331192	0.628409549	-5.065664455	4.07E-07	6.93E-05	-
evm.model.Contig1108.11	1280.1957	1.910329124	0.506735796	3.769872072	0.00016333	0.00800449	0
evm.model.Contig1109.12	19.1247126	-2.33645117	0.728317263	-3.208012888	0.00133656	0.03831875	-
evm.model.Contig1109.22	95.8250079	-1.55660362	0.556985865	-2.794691423	0.00519493	0.09732981	7.18E-20
evm.model.Contig1110.19	221.544141	-4.02709767	0.521607303	-7.720554607	1.16E-14	8.02E-11	4.34E-12
evm.model.Contig1119.22	161.923005	-2.20476017	0.580600009	-3.797382255	0.00014623	0.00737195	7.23E-07
evm.model.Contig1119.30	1070.5104	-1.7973943	0.475599523	-3.779218034	0.00015732	0.00787054	4.37E-63
evm.model.Contig1120.3	7356.40325	2.011279165	0.432749565	4.647674606	3.36E-06	0.00036697	0
evm.model.Contig1122.2	31.9684879	-1.93374914	0.674602593	-2.866501202	0.00415037	0.08451284	0

ID	baseMean	log2FoldChange	lfcSE	stat	pvalue	padj	evalue
evm.model.Contig1122.28	116.228673	-2.71986439	0.576885848	-4.714735854	2.42E-06	0.00028096	2.91E-62
evm.model.Contig1122.32	29.7288337	-2.24744058	0.675869188	-3.325259714	0.00088336	0.02805417	1.05E-27
evm.model.Contig1134.2	40.8049063	-2.81023685	0.706378257	-3.978373937	6.94E-05	0.0040827	2.41E-47
evm.model.Contig1134.29	82.1251929	-2.87157955	0.667866931	-4.299628292	1.71E-05	0.00135111	-
evm.model.Contig1135.26	36.2178616	-1.93941096	0.685287491	-2.830069109	0.0046538	0.0911021	-
evm.model.Contig1140.3	687.01985	-1.99877469	0.467800501	-4.272707454	1.93E-05	0.00146962	3.77E-177
evm.model.Contig1153.18	38.2901204	-4.1694143	0.748314039	-5.571744053	2.52E-08	7.18E-06	1.95E-81
evm.model.Contig1159.1	102.349517	-2.79534756	0.543442838	-5.14377478	2.69E-07	4.96E-05	1.21E-08
evm.model.Contig1163.7	369.551493	-1.73886474	0.448337777	-3.878470272	0.00010512	0.00564146	1.56E-121
evm.model.Contig1163.8	813.715578	-1.76019885	0.432633782	-4.068565435	4.73E-05	0.00305063	1.91E-115
evm.model.Contig1168.34	20.8148063	-2.52571197	0.715764009	-3.528693735	0.00041762	0.01582826	1.99E-15
evm.model.Contig1169.14	702.925576	-1.55791221	0.493761744	-3.155190197	0.00160394	0.04360436	4.78E-18
evm.model.Contig117.2	58.4865034	-1.91769816	0.598264788	-3.205433787	0.00134859	0.03858158	1.37E-36
evm.model.Contig1184.6	84.2822294	-1.89680867	0.565727924	-3.352863787	0.0007998	0.02616041	1.07E-157
evm.model.Contig1189.19	82.7323013	-2.69345142	0.591396042	-4.554395416	5.25E-06	0.0005297	1.29E-74
evm.model.Contig1189.20	31.1480619	-2.09850966	0.666682588	-3.14768931	0.00164567	0.04433264	-
evm.model.Contig119.8	59.2099378	-2.87867834	0.599382212	-4.802742366	1.57E-06	0.00020838	-
evm.model.Contig1192.4	21.0551099	-1.94861017	0.697858292	-2.792272007	0.00523393	0.09749669	7.41E-17
evm.model.Contig1208.9	168.869308	-1.60996816	0.555002801	-2.900828892	0.00372177	0.07862553	9.99E-139
evm.model.Contig1211.18	44.5943431	-2.97160768	0.629966838	-4.717085888	2.39E-06	0.00028074	1.52E-50
evm.model.Contig1225.32	71.0776062	-1.88833681	0.630851321	-2.993315135	0.00275965	0.0646199	2.01E-65
evm.model.Contig1238.5	225.186559	-1.64121306	0.476872556	-3.441617775	0.00057825	0.02053023	8.12E-41
evm.model.Contig1243.3	512.018536	-2.29904066	0.506977037	-4.534802355	5.77E-06	0.00056488	0
evm.model.Contig1260.7	104.077508	-2.21754499	0.622516888	-3.562224629	0.00036773	0.01435525	0
evm.model.Contig1261.9	236.716993	-1.48350875	0.463907117	-3.197857265	0.00138453	0.03923765	-
evm.model.Contig1266.27	1617.03106	2.518701167	0.507437396	4.963570255	6.92E-07	0.00010808	4.00E-108
evm.model.Contig1269.6	174.094277	2.101925495	0.567873912	3.701394709	0.00021442	0.00985277	7.40E-154
evm.model.Contig1273.23	99.0915794	-1.70866365	0.583962021	-2.925984211	0.00343368	0.07515027	6.78E-73
evm.model.Contig128.14	17.172658	-2.37297195	0.734364861	-3.231325566	0.00123218	0.03619841	7.34E-164
evm.model.Contig1281.3	467.18021	-1.93706201	0.445774723	-4.345383225	1.39E-05	0.00113689	3.39E-109
evm.model.Contig1283.9	57.9017646	-2.41455721	0.658244138	-3.668178833	0.00024428	0.0106846	0
evm.model.Contig1284.13	53.9759651	-1.9591385	0.647087811	-3.027623874	0.00246485	0.05933046	-
evm.model.Contig1295.14	48.3538975	-1.90317399	0.673692538	-2.824988973	0.00472822	0.09143875	2.60E-165
evm.model.Contig130.1	19.1313863	-2.41824915	0.737359806	-3.279605337	0.00103952	0.03193922	5.81E-50
evm.model.Contig1317.7	4346.26393	-1.64642857	0.479741438	-3.431908179	0.00059935	0.02106347	8.37E-142
evm.model.Contig1318.23	22.1898347	-1.98259263	0.687744999	-2.882743793	0.00394228	0.08147377	8.08E-16
evm.model.Contig1328.23	32.1746112	-2.29910099	0.723345986	-3.178425039	0.00148078	0.04107166	8.86E-100

ID	baseMean	log2FoldChange	lfcSE	stat	pvalue	padj	evalue
evm.model.Contig1336.2	196.474467	1.934965597	0.477056423	4.056051874	4.99E-05	0.00316041	0
evm.model.Contig1337.16	36.8498554	-2.0106677	0.655505026	-3.067356648	0.00215961	0.05344936	1.18E-78
evm.model.Contig1339.15	143.081987	-2.61786995	0.577281147	-4.534826693	5.77E-06	0.00056488	0
evm.model.Contig1339.16	168.465653	-2.24878415	0.550258559	-4.086777231	4.37E-05	0.00286591	2.15E-83
evm.model.Contig1339.17	44.049502	-2.12424045	0.636871933	-3.335427951	0.00085168	0.02721452	3.13E-115
evm.model.Contig134.7	58.6910203	-1.96387212	0.662699411	-2.963443285	0.00304218	0.06875528	0
evm.model.Contig1345.23	2860.7745	-1.72596899	0.465427455	-3.708352343	0.00020861	0.0096716	5.53E-108
evm.model.Contig1345.25	3115.42287	-1.67809652	0.459666739	-3.65068077	0.00026155	0.01130692	1.34E-85
evm.model.Contig1347.14	1341.46942	-1.64433829	0.498478935	-3.298711678	0.0009713	0.03020033	0
evm.model.Contig1351.4	119.36839	-1.75367759	0.555518864	-3.156828152	0.00159495	0.04341701	1.23E-161
evm.model.Contig1367.14	868.051702	2.223934613	0.509760734	4.36270286	1.28E-05	0.00106963	2.99E-53
evm.model.Contig1367.15	757.357075	1.770164076	0.505493333	3.501854448	0.00046203	0.01722873	9.05E-13
evm.model.Contig1378.5	33.0634204	-1.97922794	0.691115354	-2.863817061	0.0041857	0.08508711	3.65E-129
evm.model.Contig1383.14	111.524539	-2.20320012	0.61188898	-3.60065338	0.00031742	0.01285143	-
evm.model.Contig1395.4	525.502593	-2.45552749	0.507763862	-4.835963469	1.33E-06	0.00018595	3.11E-74
evm.model.Contig1397.12	53.6255458	-1.68035967	0.601628872	-2.793017011	0.00522189	0.09749669	-
evm.model.Contig14.18	2231.5854	1.677633693	0.554922252	3.023186919	0.00250128	0.05985198	1.24E-93
evm.model.Contig1402.3	196.725803	-1.86972912	0.604195002	-3.094578935	0.00197092	0.05004414	0
evm.model.Contig1403.5	966.556319	-2.75081077	0.588181294	-4.676807643	2.91E-06	0.00032713	2.88E-140
evm.model.Contig1403.6	358.955601	-2.46678606	0.485876775	-5.076978754	3.83E-07	6.75E-05	1.39E-177
evm.model.Contig1408.8	86.961564	-1.58681328	0.55819768	-2.842744317	0.00447269	0.08872765	1.34E-29
evm.model.Contig1411.12	25.7807013	-2.30933308	0.711386139	-3.246244128	0.00116939	0.0349973	4.20E-68
evm.model.Contig1412.4	25.0006078	-2.35654776	0.709605803	-3.320925153	0.0008972	0.02836341	3.68E-49
evm.model.Contig1417.2	125.751623	1.704274988	0.508066393	3.354433616	0.00079528	0.0261126	0
evm.model.Contig1423.21	4001.51303	2.382928929	0.488359528	4.879456208	1.06E-06	0.00015238	0
evm.model.Contig1424.10	14163.7028	1.533142865	0.48919574	3.134006979	0.00172437	0.04599562	-
evm.model.Contig1437.24	36.402849	-1.73957284	0.619971854	-2.80589003	0.00501778	0.09510011	0
evm.model.Contig1444.19	156.037588	-1.80421389	0.566463939	-3.185046328	0.00144731	0.04057417	-
evm.model.Contig1454.11	277.809716	-1.87600337	0.647412363	-2.897694696	0.00375916	0.07915424	-
evm.model.Contig1454.7	298.707563	-1.5341509	0.531329286	-2.887382527	0.00388462	0.08102331	1.29E-111
evm.model.Contig1472.13	37.0903357	-1.99993336	0.647849885	-3.087032058	0.00202166	0.05083515	1.63E-47
evm.model.Contig1477.15	164.278621	-1.91438536	0.521708905	-3.669451192	0.00024307	0.0106846	-
evm.model.Contig1477.16	149.188907	-1.76001015	0.523439458	-3.362394865	0.0007727	0.02559631	-
evm.model.Contig1480.12	72.0875299	-2.01365803	0.67149545	-2.99876646	0.00271075	0.06362302	0
evm.model.Contig1491.1	80.7544414	-2.5249691	0.696846834	-3.623420495	0.00029073	0.01214993	0
evm.model.Contig1497.7	189.030158	-1.86441986	0.573478925	-3.251069537	0.00114972	0.03462811	4.08E-134
evm.model.Contig1502.15	367.62347	1.557367286	0.547010989	2.847049362	0.00441265	0.08813838	-
evm.model.Contig1502.19	24.8219455	-2.49091103	0.697779662	-3.569767309	0.0003573	0.01408176	-
evm.model.Contig1515.2	225.240494	-1.6286568	0.486310969	-3.349002802	0.00081103	0.02648599	6.31E-40

ID	baseMean	log2FoldChange	lfcSE	stat	pvalue	padj	evalue
evm.model.Contig1519.5	45.6993266	-2.65795671	0.670091995	-3.966554937	7.29E-05	0.00425512	2.94E-51
evm.model.Contig1520.10	89.3150788	-1.64944346	0.576651536	-2.86038162	0.00423131	0.08565732	7.18E-32
evm.model.Contig1521.3	188.737573	-3.77527403	0.6109507	-6.179343157	6.44E-10	6.92E-07	1.03E-55
evm.model.Contig1532.5	23.0905484	2.263256983	0.725152698	3.121076416	0.00180191	0.04719512	1.47E-49
evm.model.Contig1538.2	156.458283	2.036734001	0.551136116	3.69551902	0.00021944	0.00995137	1.24E-81
evm.model.Contig1545.13	2031.21685	-1.5336397	0.520856958	-2.944454657	0.00323524	0.07209872	0
evm.model.Contig1545.14	269.487984	-1.6018839	0.507877815	-3.154073375	0.00161009	0.04371436	2.22E-44
evm.model.Contig1552.17	82.8387134	-2.03909493	0.565802201	-3.603900675	0.00031348	0.01274152	9.52E-90
evm.model.Contig1554.8	2688.16239	-1.51942527	0.530698107	-2.863068952	0.00419559	0.08510579	2.09E-153
evm.model.Contig1564.10	47.0672319	2.189379907	0.606940473	3.607239928	0.00030947	0.01262814	7.74E-151
evm.model.Contig1564.12	286.121905	3.278095928	0.555386233	5.902371603	3.58E-09	1.91E-06	3.51E-85
evm.model.Contig1609.5	23.7146134	-2.33793621	0.690406899	-3.386316414	0.00070838	0.02388471	8.53E-167
evm.model.Contig1613.15	649.150208	-1.58467713	0.495001502	-3.201358228	0.00136781	0.03897049	0
evm.model.Contig1624.16	65.7581957	-1.79154535	0.552190572	-3.244433073	0.00117685	0.03516994	-
evm.model.Contig1631.9	36.0023357	-2.89460972	0.649411356	-4.457282269	8.30E-06	0.00074633	1.06E-111
evm.model.Contig1636.3	54.9833187	-2.15475993	0.601751077	-3.580816073	0.00034252	0.01362873	5.41E-60
evm.model.Contig1637.13	182.166185	-1.69915915	0.517862084	-3.281103611	0.00103402	0.0318171	-
evm.model.Contig1641.2	43.8096021	-1.88516955	0.639612625	-2.94736138	0.00320498	0.07165503	0
evm.model.Contig165.7	68.3113963	-1.99391693	0.632357577	-3.15314784	0.0016152	0.04379595	2.00E-57
evm.model.Contig1684.8	31.2583504	-2.02115779	0.64920153	-3.113297947	0.00185009	0.04815338	1.64E-88
evm.model.Contig1685.11	346.970501	1.882131415	0.520790698	3.613988157	0.00030152	0.01245056	3.23E-107
evm.model.Contig17.47	213.821199	-2.54268804	0.535089162	-4.751895988	2.02E-06	0.00024766	1.04E-41
evm.model.Contig1707.10	24.22162	-2.05127848	0.702934903	-2.918162798	0.003521	0.07609913	3.36E-30
evm.model.Contig1729.8	2203.6463	1.951682689	0.460951022	4.234034843	2.30E-05	0.00169058	-
evm.model.Contig1761.11	393.994559	1.584100078	0.523144739	3.028034043	0.0024615	0.05933046	-
evm.model.Contig1769.2	2199.85998	-1.44516564	0.481039798	-3.004253803	0.00266233	0.06269458	2.39E-130
evm.model.Contig177.3	18.8935993	-2.26585281	0.741579053	-3.055443383	0.00224728	0.05497763	5.72E-47
evm.model.Contig177.4	26.1300103	-2.42362191	0.710221991	-3.412485034	0.00064373	0.02228395	1.36E-26
evm.model.Contig1771.7	130.307216	2.012178474	0.578989251	3.475329584	0.00051023	0.01872331	-
evm.model.Contig1773.14	142.698734	-2.74648063	0.635667754	-4.320622861	1.56E-05	0.00124772	2.27E-70
evm.model.Contig1834.4	252.829566	-3.20093584	0.546395339	-5.858278072	4.68E-09	2.02E-06	2.85E-25
evm.model.Contig1837.11	201.950654	-1.6162764	0.571387783	-2.828685609	0.00467396	0.09117432	0
evm.model.Contig1851.10	2757.09768	-1.30115156	0.450473115	-2.888411128	0.00387193	0.08090551	2.08E-80
evm.model.Contig1851.7	128.129286	1.53114637	0.530336039	2.887124876	0.0038878	0.08102331	-
evm.model.Contig1870.4	22.302526	-2.37495155	0.703431701	-3.376236163	0.00073485	0.02461741	1.52E-07
evm.model.Contig1882.11	74.576093	-1.77643728	0.636832699	-2.789488164	0.00527914	0.09816275	8.28E-16
evm.model.Contig1896.12	1834.53263	2.104878066	0.530077142	3.970890084	7.16E-05	0.00420121	0
evm.model.Contig1899.11	59.5835434	-2.97313488	0.592281281	-5.019802197	5.17E-07	8.46E-05	5.40E-100
evm.model.Contig1918.4	735.913564	-1.6956529	0.600027219	-2.825959976	0.00471392	0.09143875	-

ID	baseMean	log2FoldChange	lfcSE	stat	pvalue	padj	evalue
evm.model.Contig1957.10	73.8697042	-2.02280116	0.694044203	-2.914513441	0.00356243	0.07675495	2.69E-17
evm.model.Contig1964.2	29.1660978	-2.65423063	0.718808225	-3.692543484	0.00022202	0.01002479	6.33E-85
evm.model.Contig1967.3	68.0096142	-1.91767573	0.622437502	-3.080912895	0.00206367	0.05170377	3.30E-41
evm.model.Contig199.6	1321.58643	1.427392111	0.490531116	2.909891063	0.00361555	0.0775774	0
evm.model.Contig2006.4	204.490992	-1.82587349	0.586752237	-3.111830463	0.00185931	0.04821213	4.15E-50
evm.model.Contig2016.6	172.565208	-2.06874989	0.5877744	-3.519632511	0.00043215	0.01626024	3.23E-71
evm.model.Contig2018.9	3980.36551	-1.24576082	0.436253407	-2.855589891	0.0042957	0.08645505	0
evm.model.Contig2024.9	61.9884033	-3.46850141	0.615562768	-5.634683569	1.75E-08	5.28E-06	7.51E-07
evm.model.Contig2032.6	173.729797	-2.08009454	0.541097912	-3.844210984	0.00012094	0.0062956	1.98E-21
evm.model.Contig2045.7	421.784858	-1.36142364	0.477783008	-2.849460156	0.00437935	0.08778826	3.18E-135
evm.model.Contig2083.7	107.05167	-2.15754805	0.522158399	-4.13197997	3.60E-05	0.00248782	4.49E-41
evm.model.Contig2083.8	881.193434	-2.53843525	0.452662687	-5.607785507	2.05E-08	5.99E-06	9.80E-88
evm.model.Contig2110.1	178.379603	-2.40741301	0.614403565	-3.918292715	8.92E-05	0.00492616	4.04E-103
evm.model.Contig2134.11	129.978218	-2.33214961	0.580028729	-4.020748438	5.80E-05	0.00353753	1.08E-22
evm.model.Contig219.3	5446.21004	-2.96736171	0.502267791	-5.907927526	3.46E-09	1.89E-06	0
evm.model.Contig219.6	69.4954852	-2.352319	0.586310149	-4.012072797	6.02E-05	0.00364462	9.31E-46
evm.model.Contig2206.4	54.4881361	-2.16880437	0.593804274	-3.652389285	0.00025981	0.01126574	6.20E-22
evm.model.Contig2217.3	237.703624	-3.36573865	0.591599276	-5.689220358	1.28E-08	4.08E-06	3.79E-25
evm.model.Contig2218.1	215.051268	-3.33328132	0.532205053	-6.263152338	3.77E-10	4.61E-07	6.24E-14
evm.model.Contig226.8	39.0945468	-1.8317318	0.62908051	-2.91176053	0.00359398	0.0772743	-
evm.model.Contig2260.2	183.628636	-3.09619483	0.593078952	-5.220544112	1.78E-07	3.50E-05	7.69E-11
evm.model.Contig2320.1	164.397484	-2.79175171	0.669059812	-4.172648928	3.01E-05	0.00212701	0
evm.model.Contig2331.4	116.704343	-3.74927522	0.578344474	-6.482771753	9.01E-11	1.70E-07	4.39E-31
evm.model.Contig2363.8	44.8856789	-1.94777826	0.637179101	-3.0568772	0.00223656	0.05477987	1.56E-43
evm.model.Contig2370.2	630.831772	-1.55001123	0.446203487	-3.473776597	0.00051319	0.01873272	1.71E-82
evm.model.Contig2401.4	27.9411053	-3.08600633	0.758714425	-4.067414868	4.75E-05	0.00305063	3.50E-150
evm.model.Contig2435.5	839.035775	-1.72763166	0.48698304	-3.547621831	0.00038873	0.01501175	1.52E-149
evm.model.Contig2445.6	30.1136783	-2.4736451	0.655037644	-3.776340363	0.00015915	0.0078891	7.72E-26
evm.model.Contig2528.4	120.530333	1.901276743	0.540186198	3.519669239	0.00043209	0.01626024	9.25E-36
evm.model.Contig253.3	30.458879	-2.23545212	0.757548442	-2.9509032	0.00316846	0.07099132	2.88E-120
evm.model.Contig2531.2	1413.52755	-2.05394429	0.500651462	-4.102543285	4.09E-05	0.0027116	0
evm.model.Contig2554.1	29.4713156	-2.06601306	0.692596254	-2.982997741	0.0028544	0.06594651	1.50E-14
evm.model.Contig2559.3	62.0688002	-1.85902764	0.624736988	-2.975696448	0.00292324	0.06716339	7.32E-53
evm.model.Contig2591.1	99.3631788	-2.65478436	0.534713492	-4.964872594	6.87E-07	0.00010808	1.02E-42
evm.model.Contig2625.2	17.0211575	-2.39504858	0.765869636	-3.127227486	0.00176463	0.04674928	4.01E-84
evm.model.Contig266.2	309.395182	1.657534589	0.51133765	3.241565702	0.00118875	0.03527192	5.89E-11
evm.model.Contig2708.1	53.3981819	-1.87391991	0.599163343	-3.127561008	0.00176263	0.04674928	0
evm.model.Contig2722.2	846.813202	-1.94869673	0.465009746	-4.190657815	2.78E-05	0.00200594	3.25E-142
evm.model.Contig277.3	613.602069	1.717144418	0.519537142	3.305142749	0.00094928	0.02956005	-

ID	baseMean	log2FoldChange	lfcSE	stat	pvalue	padj	evalue
evm.model.Contig278.12	93.2885778	-1.99454318	0.539040591	-3.700172523	0.00021545	0.00987849	-
evm.model.Contig2868.3	15.5510559	-2.20103335	0.75908374	-2.89959228	0.00373648	0.07878859	3.96E-127
evm.model.Contig294.4	1072.98948	1.748140159	0.501157205	3.488207179	0.00048627	0.0180033	5.61E-68
evm.model.Contig3048.3	93.4509257	1.720385475	0.569277843	3.022048892	0.0025107	0.06000833	-
evm.model.Contig31.37	14.3060425	-2.59546063	0.764687966	-3.394143417	0.00068844	0.02344069	0
evm.model.Contig316.4	139.785697	2.209450305	0.548816796	4.025843087	5.68E-05	0.00350936	1.49E-171
evm.model.Contig322.1	111.688603	-3.18174274	0.610753669	-5.209535201	1.89E-07	3.64E-05	9.72E-149
evm.model.Contig3247.2	296.269854	1.505666351	0.53915481	2.79264197	0.00522795	0.09749669	-
evm.model.Contig3277.1	96.2556025	-2.38574551	0.631156577	-3.779958253	0.00015685	0.00786925	2.22E-31
evm.model.Contig3378.2	1882.87953	-2.24751814	0.455658766	-4.932458904	8.12E-07	0.00012133	4.53E-67
evm.model.Contig34.1	23.5652212	-2.51957481	0.730829198	-3.447556301	0.00056568	0.02023273	0
evm.model.Contig3406.3	17.5889353	-2.0705215	0.73022685	-2.835449692	0.00457612	0.08983559	-
evm.model.Contig3459.1	15.8048835	-2.28607112	0.769475242	-2.970948243	0.00296882	0.06776083	4.38E-28
evm.model.Contig35.3	411.004718	-1.6571569	0.481926874	-3.438606548	0.00058472	0.0206892	1.78E-161
evm.model.Contig3512.1	211.44787	-1.73911548	0.486124162	-3.577512943	0.00034688	0.01374939	3.38E-95
evm.model.Contig3515.2	1618.38986	2.071287242	0.495767261	4.177942764	2.94E-05	0.00208521	0
evm.model.Contig3670.2	527.889904	1.819080263	0.537077333	3.386998763	0.00070662	0.02386412	3.69E-31
evm.model.Contig378.2	274.977349	-2.33363404	0.64041518	-3.643939291	0.0002685	0.01151645	1.17E-91
evm.model.Contig3852.1	744.075914	2.733777417	0.517385517	5.283830581	1.27E-07	2.80E-05	7.44E-48
evm.model.Contig3936.2	192.224326	-1.99851185	0.521385795	-3.83307691	0.00012655	0.00657113	4.11E-43
evm.model.Contig3964.1	1642.15103	2.478484978	0.5233183	4.736094609	2.18E-06	0.0002631	1.42E-37
evm.model.Contig4034.2	50.8866054	-1.89185101	0.649391263	-2.91326835	0.00357667	0.07698182	1.73E-25
evm.model.Contig4038.1	67.4299675	-2.22665555	0.611497406	-3.641316422	0.00027125	0.0115684	9.49E-47
evm.model.Contig4143.1	24.3156323	-1.94419535	0.689147862	-2.821158505	0.00478506	0.09219443	-
evm.model.Contig4159.1	73.4312573	2.110144707	0.584141943	3.612383481	0.0003034	0.01247826	-
evm.model.Contig4176.1	109.831141	-2.35353849	0.600907161	-3.916642435	8.98E-05	0.00494683	4.93E-17
evm.model.Contig4288.2	82.1125846	-2.16616918	0.637659931	-3.397060218	0.00068114	0.02326854	6.48E-153
evm.model.Contig4428.2	1276.7922	-1.40495461	0.447616844	-3.13874383	0.00169674	0.04541395	4.89E-48
evm.model.Contig4432.1	160.925481	-2.97604515	0.647179761	-4.59848304	4.26E-06	0.00044326	1.59E-09
evm.model.Contig4441.2	120.813778	-1.56254719	0.529073368	-2.9533658	0.00314329	0.07050344	1.66E-82
evm.model.Contig448.2	1747.62935	-1.56694042	0.482001191	-3.250905699	0.00115038	0.03462811	1.96E-43
evm.model.Contig448.3	1070.26541	-1.56750084	0.485369607	-3.229499361	0.00124007	0.03637894	1.57E-43
evm.model.Contig454.3	24.5944049	-2.42087897	0.723638923	-3.34542393	0.00082157	0.02666248	3.63E-14
evm.model.Contig457.1	49.5649631	-1.67439586	0.596109933	-2.808870929	0.00497156	0.09464642	-
evm.model.Contig4801.1	94.0743422	-1.98446294	0.618637312	-3.207797035	0.00133756	0.03831875	9.15E-94
evm.model.Contig4989.1	16.6606141	-2.47735112	0.773633246	-3.202229392	0.00136368	0.03895971	1.09E-10
evm.model.Contig508.1	406.416118	1.705784711	0.471005969	3.621577692	0.00029281	0.01215787	1.92E-56
evm.model.Contig511.3	277.463432	-1.65501019	0.545094825	-3.036187683	0.0023959	0.05793118	0
evm.model.Contig5228.1	58.5016441	1.882937798	0.60901306	3.091785584	0.00198957	0.05027161	0
evm.model.Contig5545.1	170.130073	-1.66151781	0.493970961	-3.363594095	0.00076935	0.02554302	1.02E-36

ID	baseMean	log2FoldChange	lfcSE	stat	pvalue	padj	evalue
evm.model.Contig5706.1	46.3466002	-2.0566933	0.650630588	-3.161076874	0.00157187	0.04306722	-
evm.model.Contig58.28	74.8541583	-1.80396905	0.572884963	-3.14892023	0.00163875	0.04420366	2.82E-111
evm.model.Contig5896.1	36.2767599	-2.39050618	0.688560806	-3.471743034	0.00051709	0.01884207	-
evm.model.Contig6.36	308.848266	2.934767043	0.544461276	5.390221804	7.04E-08	1.70E-05	4.36E-84
evm.model.Contig6000.1	19.7435311	-2.18825977	0.749058012	-2.921348857	0.00348519	0.0756893	-
evm.model.Contig6213.2	59.7601478	-1.94543863	0.604190239	-3.219910717	0.00128231	0.0371976	-
evm.model.Contig6486.2	19.5478356	-2.40674638	0.741363458	-3.24637848	0.00116883	0.0349973	5.13E-139
evm.model.Contig66.10	44.4755042	-2.650071	0.659142405	-4.020483245	5.81E-05	0.00353753	2.50E-86
evm.model.Contig6678.1	57.572753	-2.34679259	0.634926039	-3.696166876	0.00021888	0.00995137	1.62E-112
evm.model.Contig6678.2	79.5132124	-2.45230438	0.580537851	-4.224193789	2.40E-05	0.00175603	5.98E-81
evm.model.Contig725.1	788.148201	-1.74324231	0.515977983	-3.378520733	0.00072877	0.02445321	2.06E-78
evm.model.Contig782.3	1010.65394	-1.3845033	0.466967102	-2.964884031	0.00302797	0.06850866	-
evm.model.Contig789.16	226.690765	-3.16897989	0.596273055	-5.31464547	1.07E-07	2.39E-05	1.55E-123
evm.model.Contig791.41	182.938028	1.396968708	0.479301681	2.914591715	0.00356154	0.07675495	4.23E-11
evm.model.Contig813.44	520.690727	1.447750877	0.449529794	3.220589371	0.00127927	0.03718606	0
evm.model.Contig813.45	1653.66872	1.247578443	0.432829596	2.882377857	0.00394686	0.08148738	0
evm.model.Contig818.42	38.3868709	-2.27235233	0.699358105	-3.249197104	0.00115731	0.03478637	5.73E-37
evm.model.Contig820.15	33.8726569	-1.88701184	0.671772185	-2.80900561	0.00496948	0.09464642	-
evm.model.Contig820.4	70.5132788	-1.71143826	0.603228446	-2.837131233	0.00455209	0.08961792	6.80E-122
evm.model.Contig821.24	3626.78443	-1.22246245	0.430095931	-2.842301827	0.00447891	0.08876612	0
evm.model.Contig821.28	554.181023	-2.0101871	0.500872003	-4.013374861	5.99E-05	0.00363516	0
evm.model.Contig826.28	21.4146645	-3.73333385	0.756399368	-4.935664954	7.99E-07	0.00012043	2.60E-99
evm.model.Contig829.2	14.5135621	-2.09992662	0.74576694	-2.815794738	0.00486567	0.09325484	-
evm.model.Contig837.11	27.95409	-1.97111126	0.701558104	-2.809619405	0.00496001	0.09460004	-
evm.model.Contig843.27	28.151436	-2.79341343	0.693336064	-4.028945807	5.60E-05	0.00347371	-
evm.model.Contig844.9	180.087178	-2.18451715	0.626602489	-3.486288657	0.00048977	0.01806851	2.57E-108
evm.model.Contig849.9	372.844043	-2.01341858	0.481129309	-4.184776406	2.85E-05	0.00205146	5.23E-69
evm.model.Contig871.27	279.739578	1.512276148	0.515096297	2.93590957	0.00332571	0.07332808	0
evm.model.Contig871.28	630.414707	1.511301039	0.494310102	3.057394603	0.0022327	0.05477485	0
evm.model.Contig871.29	805.570464	1.41160628	0.487399731	2.896198316	0.00377714	0.07940397	0
evm.model.Contig871.45	19.850374	-2.70160374	0.735049839	-3.675402121	0.00023748	0.01051675	1.41E-26
evm.model.Contig872.9	395.200039	-1.91586911	0.491979174	-3.894207748	9.85E-05	0.00532881	4.11E-94
evm.model.Contig874.8	251.595716	2.798204966	0.532088927	5.25890471	1.45E-07	3.04E-05	1.20E-117
evm.model.Contig879.7	332.605064	-1.63906722	0.49283416	-3.325798729	0.00088166	0.02804286	7.31E-44
evm.model.Contig885.26	571.501799	-1.90699472	0.461811424	-4.129379699	3.64E-05	0.00249338	3.48E-07
evm.model.Contig885.8	54.9849504	-1.98609904	0.652066705	-3.045852555	0.00232022	0.05662853	-
evm.model.Contig886.29	1130.29704	2.313183192	0.513592751	4.503924926	6.67E-06	0.00063056	-
evm.model.Contig889.35	174.275822	-2.44248425	0.534813288	-4.566984973	4.95E-06	0.00050131	3.19E-43
evm.model.Contig897.22	107.421905	-1.86379845	0.612171208	-3.044570587	0.00233013	0.0567371	1.10E-103

ID	baseMean	log2FoldChange	lfcSE	stat	pvalue	padj	evalue
evm.model.Contig903.15	26.5493792	-1.925644	0.681743341	-2.824587915	0.00473415	0.0914681	3.21E-31
evm.model.Contig903.31	16.0601755	-2.53240334	0.755026643	-3.35405825	0.00079636	0.0261126	0
evm.model.Contig909.12	177.374112	2.630324052	0.563222762	4.670130944	3.01E-06	0.00033433	3.38E-48
evm.model.Contig911.10	82.2710486	-2.14094848	0.658476029	-3.251368889	0.00114851	0.03462811	-
evm.model.Contig913.23	39.8883511	-2.20400197	0.631006656	-3.492834738	0.00047792	0.01772579	9.88E-29
evm.model.Contig913.45	21.8110882	-2.55992301	0.738607486	-3.465877421	0.0005285	0.01912375	9.53E-79
evm.model.Contig914.24	44.7114594	-1.8221385	0.648531576	-2.809637282	0.00495974	0.09460004	1.59E-53
evm.model.Contig914.25	30.2226696	-2.17254004	0.708827514	-3.064977018	0.00217687	0.05369778	0
evm.model.Contig914.49	271.737279	-2.04943819	0.571686902	-3.584896181	0.00033721	0.01346904	-
evm.model.Contig917.4	160.280888	-2.69913548	0.511330052	-5.278656069	1.30E-07	2.85E-05	1.39E-12
evm.model.Contig92.21	1166.08938	2.747374389	0.491867556	5.585597896	2.33E-08	6.72E-06	0
evm.model.Contig920.3	260.558426	2.034445656	0.516498822	3.938916352	8.19E-05	0.00467042	-
evm.model.Contig937.6	308.51348	2.503903849	0.528082286	4.7415032	2.12E-06	0.00025767	8.00E-20
evm.model.Contig939.26	143.908999	-2.4480196	0.513262715	-4.769525476	1.85E-06	0.00023245	5.89E-28
evm.model.Contig940.27	108.165026	-2.32129259	0.637288037	-3.642454363	0.00027005	0.01154106	1.42E-72
evm.model.Contig946.19	1066.85162	-1.54870848	0.446153117	-3.471248811	0.00051804	0.01884373	-
evm.model.Contig953.21	153.092493	-3.47246569	0.60297117	-5.758924903	8.47E-09	2.98E-06	2.79E-07
evm.model.Contig954.1	577.199042	-3.30869011	0.571673831	-5.787723569	7.13E-09	2.60E-06	9.82E-156
evm.model.Contig955.19	2857.53204	2.555868131	0.504388733	5.067258574	4.04E-07	6.93E-05	-
evm.model.Contig961.28	98.6664514	-3.24958036	0.595355391	-5.458219432	4.81E-08	1.31E-05	4.36E-37
evm.model.Contig961.4	125.080999	1.886001503	0.570099333	3.308198052	0.00093898	0.02932736	0
evm.model.Contig965.35	47.9979203	-1.70453544	0.604959589	-2.817602143	0.00483837	0.09304907	-
evm.model.Contig970.31	26.9099272	-2.10329272	0.664803905	-3.163779133	0.00155735	0.04272939	1.92E-17
evm.model.Contig973.11	54.0600898	-1.70219699	0.582546555	-2.921993057	0.00347799	0.07564179	5.91E-47
evm.model.Contig973.7	636.100241	-1.69725598	0.449689895	-3.774280889	0.00016047	0.00791677	2.40E-40
evm.model.Contig980.3	49.9800199	-2.49756897	0.684318702	-3.649716077	0.00026253	0.01130864	1.70E-86